Hindawi
Cellular Microbiology
Volume 2024, Article ID 8896219, 19 pages
https://doi.org/10.1155/2024/8896219

Research Article

Dual Control of Host Actin Polymerization by a *Legionella* Effector Pair

M. Pillon,[1] **C. Michard**,[1] **N. Baïlo**,[1] **J. Bougnon**,[1,2] **K. Picq**,[3] **O. Dubois**,[1] **C. Andrea**,[1] **L. Attaiech**,[3] **V. Daubin**,[2] **S. Jarraud**,[1] **E. Kay**,[1] **and P. Doublet**[1]

[1]*CIRI, Centre International de Recherche en Infectiologie, (Team: Legionella Pathogenesis), Univ Lyon, Inserm, U1111, Université Claude Bernard Lyon 1, CNRS, UMR5308, ENS de Lyon, F-69007 Lyon, France*
[2]*Laboratoire de Biométrie et Biologie Evolutive, Univ Lyon, Université Claude Bernard Lyon 1, CNRS, UMR5558, F-69622 Villeurbanne, France*
[3]*CIRI, Centre International de Recherche en Infectiologie, (Team: HORIGENE), Univ Lyon, Inserm, U1111, Université Claude Bernard Lyon 1, CNRS, UMR5308, ENS de Lyon, F-69007 Lyon, France*

Correspondence should be addressed to P. Doublet; patricia.doublet@univ-lyon1.fr

C. Michard and N. Baïlo contributed equally to this work.

Received 16 May 2023; Revised 20 November 2023; Accepted 11 December 2023; Published 27 January 2024

Academic Editor: Sanket Kaushik

Host actin cytoskeleton is often targeted by pathogenic bacteria through the secretion of effectors. *Legionella pneumophila* virulence relies on the injection of the largest known arsenal of bacterial proteins, over 300 Dot/Icm type 4 secretion system effectors, into the host cytosol. Here, we define the functional interactions between VipA and LegK2, two effectors with antagonistic activities towards actin polymerization that have been proposed to interfere with the endosomal pathway. We confirmed the prominent role of LegK2 effector in *Legionella* infection, as the deletion of *legK2* results in defects in the inhibition of actin polymerization at the *Legionella*-containing vacuole, as well as in endosomal escape of bacteria and subsequent intracellular replication. More importantly, we observed the restoration of the *ΔlegK2* mutant defects, upon deletion of *vipA* gene, making LegK2/VipA a novel example of effector-effector suppression pair that targets the actin cytoskeleton and whose functional interaction impacts *L. pneumophila* virulence. We demonstrated that LegK2 and VipA do not modulate each other's activity in a "metaeffector" relationship. Instead, the antagonistic activities of the LegK2/VipA effector pair would target different substrates, Arp2/3 for LegK2 and G-actin for VipA, to temporally control actin polymerization at the LCV and interfere with phagosome maturation and endosome recycling, thus contributing to the intracellular life cycle of the bacterium. Strikingly, the functional interaction between LegK2 and VipA is consolidated by an evolutionary history that has refined the best effector repertoire for the benefit of *L. pneumophila* virulence.

1. Introduction

Actin cytoskeleton, including actin itself (globular, filamentous, and its polymerization) as well as accessory proteins such as myosins, is a preferential target for pathogenic bacteria [1–3]. It is a complex and dynamic network that shapes the cell and plays a key role in numerous cellular processes such as cell migration, adhesion, internalization, and intracellular trafficking. Intracellular bacteria evolved effective mechanisms that take advantage of actin polymerization in order (i) to gain entry into epithelial cells [4–7], (ii) to promote their movement within the host cytosol, thus contributing to their evasion from autophagy and their propagation to neighboring cells [8, 9], and (iii) to stabilize their replicative vacuole in epithelial cells [10, 11]. Actin polymerization inhibition or actin degradation strategies have also been described to contribute to bacterial evasion from phagocytosis [12] and to cell cytotoxicity and therefore pathogenesis development [13].

Legionella pneumophila, the etiological agent of the severe pneumonia legionellosis, is a typical example of intracellular pathogen that has evolved several mechanisms to take advantage of the host actin cytoskeleton. This sophisticated relationship allows the pathogen to achieve intracellular replication within phagocytic cells such as amoebae in aquatic environment or alveolar macrophages in its accidental human host. Intracellular replication occurs in a rough endoplasmic reticulum-like compartment called *Legionella*-containing vacuole (LCV) that evades endocytic maturation. The type 4 secretion system (T4SS) Dot/Icm is crucial for *Legionella* intracellular replication, through the secretion of over 300 effectors into the host cell cytoplasm. To date, five Dot/Icm effectors have been shown to interfere with actin polymerization, activating it for VipA and inhibiting it for the others. Specifically, VipA is an actin nucleator, which localizes to early endosomes during infection and promotes actin polymerization *in vitro* [14]; Ceg14 cosediments with F-actin and inhibits actin polymerization by an unknown mechanism [15]; LegK2 is a Ser/Thr kinase that phosphorylates ArpC1b and Arp3, two subunits of the Arp2/3 complex, thus inhibiting actin polymerization on the LCV and contributing to the bacterial evasion from endosomal degradation [16]; RavK is a metalloprotease that cleaves actin, generating a fragment with a diminished capacity to form actin filaments [17]; and WipA is a phosphotyrosine phosphatase that disrupts F-actin polymerization by hijacking phosphotyrosine signaling [18].

We sought to establish the functional interactions between VipA and LegK2, as both effectors exhibit antagonistic activities towards actin polymerization and both have been proposed to interfere with the endosomal pathway [14, 16]. We constructed and characterized simple and double mutants with in-frame deletion of the genes encoding these effectors. We confirmed the role of LegK2 in the inhibition of actin polymerization on the LCV. More importantly, we observed the restoration of the *ΔlegK2* mutant defect in this step, upon deletion of *vipA*, thus identifying the first *Legionella* effector-effector suppression pair targeting the host cell actin cytoskeleton. By doing so, we proposed for the first time a role for VipA in the infectious cycle of *L. pneumophila*. Strikingly, the compensation of the *legK2* phenotype by *vipA* deletion was also shown for bacterial escape from the endosomal pathway as well as for intracellular replication, thus making LegK2/VipA the first example of effector-effector suppression pair whose functional interaction impacts *L. pneumophila* virulence. We demonstrated that LegK2 and VipA differ from other effector-effector suppression pairs identified by targeted functional studies or systematic screens [19], in that these effectors do not exhibit antagonistic enzymatic activities against a common substrate and do not modulate the other's activity in a metaeffector-effector relationship. Rather, they target different components of the actin cytoskeleton, to contribute to the intracellular life cycle of the bacteria. Finally, combined with the phylogenetic study of the genes encoding LegK2 and VipA, this work shows that the functional interaction between two Dot/Icm effectors results from an evolutionary history that has refined the best effector repertoire for the benefit of *L. pneumophila* virulence.

2. Materials and Methods

2.1. Cell Lines and Bacterial Strains. Bacterial strains and cell lines used in this study are summarized in Supplementary Data S1.

L. pneumophila strains were grown at 37°C either in BCYE (buffered charcoal yeast extract) agar or in AYE (ACES ([*N*-(2-acetamido)-2-aminoethanesulfonic acid] yeast extract) liquid medium (12 g/L yeast extract (Difco), 10 g/L ACES (Roth), 0.4 g/L L-cysteine HCl (Euromedex), 0.25 g/L, pH adjusted to 6.9 with KOH 1 N). Each medium was supplemented with 5 μg/ml chloramphenicol and isopropyl-β-d-thiogalactopyranoside (IPTG) 1 mM or 500 μM when appropriate.

E. coli strains were grown at 37°C in LB medium supplemented with 100 μg/ml ampicillin and 20 μg/ml kanamycin. *E. coli* strains DH5α were used to maintain plasmids used for transfection in HeLa cells. The WT amoeba *D. discoideum* strains Ax2 (DBS0235534) and calnexin-GFP (DBS0236184) were obtained from the Dicty Stock Center (http://dictybase.org). *D. discoideum* cells were grown axenically in HL5 medium at 22°C with 100 μg/ml streptomycin and 66 μg/ml penicillin G and for calnexin-GFP strain with 20 μg/ml neomycin. The *A. castellanii* environmental isolate (gift from P. Pernin from Laboratory of Pharmacy, Université Lyon 1, Lyon, France) was grown axenically in PYg medium at 30°C with 100 μg/ml streptomycin and 66 μg/ml penicillin G.

HeLa cells (gift from INSERM U1111, Lyon, France) were maintained at 37°C in 5% CO_2 in DMEM (Dulbecco's modified Eagle's medium) supplemented with 10% heat-inactivated fetal calf serum (FCS). U937 monocyte cells were maintained at 37°C in 5% CO_2 in RPMI 1640 medium (ThermoFisher Scientific) supplemented with 10% heat-inactivated foetal calf serum (HyClone™). U937 monocyte differentiation into macrophages is conducted during 2 days at a phorbol 12-myristate 13-acetate (PMA) concentration of 100 ng/ml.

2.2. General Cloning Techniques. The plasmids and primers used in this study are shown in Supplementary Data S2 and S3. Gateway cloning technic was performed for cloning into mammalian expression vectors as recommended by the manufacturer (Invitrogen). SLIC cloning was performed following the procedure described by Li and Elledge [20] for cloning into bacterial expression vectors. Restriction enzymes, T4 DNA ligase, and T4 DNA polymerase were purchased from New England Biolabs. Plasmid DNA from *E. coli* was extracted by Plasmid Midi and Mini Kits (Omega). PCR amplifications were carried out with PrimeStar polymerase as recommended by the manufacturer (Takara). *E. coli* competent cells are transformed by thermal shock with 100 ng of plasmid DNA, and *L. pneumophila* strains are transformed by electroporation (2.4 kV, 100 Ω and 25 μF) with 2 μg of plasmid DNA.

DNA fragments corresponding to the *legK2* (*lpp2076*) and *vipA* (*lpp0457*) coding sequences were amplified by PCR using genomic DNA of *L. pneumophila* Paris as a template and specific primers as described in Supplementary

Data S3. The coding sequences were inserted into the Gateway pDONR207 vector (Invitrogen) by *in vitro* recombination. The *legK2* and *vipA*-encoding genes were transferred by Gateway cloning from pDONR207-*legK2* and pDONR207-*vipA* to vectors pDEST27 and peGFP (Invitrogen) to produce GST-tagged LegK2 and C or N-terminal GFP-fused VipA proteins in mammalian cells, respectively. The coding sequences amplified by primers were also inserted into the XmaI-linearized pXDC61 vector by SLIC cloning to produce β-lactamase-fused LegK2 or VipA proteins.

2.3. Gene Inactivation and Translational Fusions Insertion in L. pneumophila. A homologous recombination strategy was performed as previously described [21] in order to obtain *L. pneumophila* Paris mutant strains for *lpp2076* and *lpp0457* genes. The 2000-bp upstream and downstream regions of the gene of interest were amplified by PCR with primers carrying 30-nt sequences (P1-P2 primers pair for the upstream region; P3-P4 primers pair for the downstream region) complementary to a counter-selectable mazF-kan (MK) cassette (Supplementary Data S3). The upstream and downstream regions were assembled to the MK cassette (amplified from plasmid pGEM-mazF-kan with MazFk7-F/MazF-R primers) by PCR overlap extension and used for the natural transformation of *Legionella* strains. Transformants were then selected on CYE+kanamycin and counter-selected for sensitivity on CYE+IPTG. Integration of the cassette at the correct locus was also verified by PCR. To obtain scar-free mutants, a second step was performed as follows. Upstream and downstream regions of each gene of interest were amplified with primers carrying a 20-nt tail sequence corresponding to the 3′ end of upstream and downstream region (P1-P5 primers pair for upstream and P4-P6 primer pair for downstream region, Supplementary Data S3), respectively, and were assembled by PCR overlap extensions. For translational fusions, the *luc* and SF-*gfp* genes were amplified and assembled with the gene of interest by PCR extension. Theses PCRs were used to transform the previous *Δlpp2076*::mazF-kan or *Δlpp0457*::mazF-kan strains. Transformants were then selected on CYE+IPTG and counter-selected for sensitivity on CYE+Kan. Scar-free deletion of *lpp2076* and *lpp0457* genes and translational fusions were verified by PCR and sequencing.

2.4. Intracellular Growth Kinetics in A. castellanii or U937 Macrophages. L. pneumophila cells harbouring a fluorescent mCherry protein-producing plasmid were grown on BCYE agar containing 1 M IPTG and 0.5 μg/mL chloramphenicol for 24 hours at 37°C. *A. castellanii* cells were plated in 96-well microplates (10^5 cells/well) in PY special medium (16 mM $MgSO_4$, 40 mM $CaCl_2$, 3.4 mM sodium citrate dihydrate, 50 μM $Fe(NH_4)2(SO_4)2$, 2.5 mM Na_2HPO_4, 2.5 mM KH_2PO_4) and infected at MOI = 5. Infection was synchronized by spinning the infected plates at 2500 rpm for 10 min. Intracellular growth was automatically monitored by measuring mCherry fluorescence at $\lambda_{ex} = 587$ nm and $\lambda_{em} = 610$ nm on an Infinite M200 microplate reader (Tecan) or by lysing infected amoebae with 0.8% saponin, plating lysates at different dilutions on BCYE agar plates and counting grown bacteria at day 4 postplating.

U937 macrophages were plated and differentiated in 96-well microplates (10^5 cells/well) in RPMI+10% FBS +PMA medium and infected at MOI = 1. Infection was synchronized by spinning the infected plates at 2500 rpm for 10 min. Intracellular growth was monitored by lysing infected macrophages with sterile water, plating lysates at different dilutions on BCYE agar plates, and counting grown bacteria at day 4 postplating.

2.5. D. discoideum Infection by L. pneumophila for Microscopic Analysis. D. discoideum cells were plated at a concentration of 5×10^5 cells/mL on sterile glass coverslips a day before infection in MB medium (7.15 g/L yeast extract; 14.3 g/L peptone; 20 mM MES and buffered at a pH 6.9) and incubated overnight at 22°C. Monolayers were infected the next day at an MOI of 100 with mCherry-expressing bacteria grown overnight at 37°C in AYE 1X medium supplemented with chloramphenicol and IPTG for maintenance and induction of mCherry expression plasmid pXDC50. Plates were then spun at 2000 rpm for 10 min, incubated at 25°C for a specific time of infection, and further treated for microscopic analysis.

2.6. v-ATPase Visualization on LCVs in D. discoideum during Infection by L. pneumophila. D. discoideum cells plated on sterile glass coverslips were infected as described above and incubated at 25°C for 1 hour. Monolayers were fixed with 4% formaldehyde, permeabilized with 0.1% Triton X-100 for 5 min at RT, and blocked in 0.2% BSA for 1 h at RT. v-ATPase was then stained with anti-VatA antibodies (gift of F. Letourneur, Montpellier, France) and detected with anti-mouse secondary antibody from goat conjugated with the fluorochrome Alexa Fluor 488 (A11029; Molecular Probes). Glass slides were then mounted on slides with Fluoromount (Thermofisher), and microscopy was carried out using a confocal laser scanning microscope (LSM800; Zeiss).

2.7. Actin Polymerization in D. discoideum during Infection by L. pneumophila. D. discoideum cells plated on sterile glass coverslips were infected as described above and incubated at 25°C for 15 min. Monolayers were fixed with 4% formaldehyde, permeabilized with 0.1% Triton X-100 for 5 min at RT, and blocked in 0.2% BSA for 1 h at RT. Actin was then stained with phalloidin-FITC (P5282; Sigma). Glass slides were then mounted on slides with Fluoromount (Thermofisher), and microscopy was carried out using a confocal laser scanning microscope (LSM800; Zeiss).

2.8. RNA Isolation and Depletion of rRNA and RNAseq. L. pneumophila Paris WT strain was grown at 37°C in AYE medium and harvested by centrifugation (5 min, 7000 rpm, 4°C) at different growth phases: at the exponential phase (optical density of 1.5 at 600 nm (OD_{600nm} 1.5)), postexponential phase (OD_{600nm} 4 and visual check of motility acquisition), and to the onset of stationary growth phase (OD_{600nm} 5). Total RNA from bacterial cultures was extracted according to a previously described procedure

[22]. Briefly, pellets of 10^9 bacterial cells were lysed in 50 μl of RNAsnap buffer (18 mM EDTA, 0.025% SDS, 95% formamide), and total RNAs were extracted using a tri-reagent solution (acid guanidinium thiocyanate–phenol–chloroform) and isopropanol-precipitated. After precipitation, we performed an additional step of RNA purification on silica-based columns (DirectZol kit, ZymoResearch) by following the manufacturer's recommendations. RNA sample purity and concentration were determined by spectrophotometric analysis on a NanoDrop 2000 UV-Vis spectrophotometer (Thermo). RNA sequencing was performed following ribosomal RNA depletion and cDNA library preparation on an NovaSeq platform (Illumina) with paired-end 150 bp (Genewiz-Azenta, Leipzig, Germany). After mapping sequence reads to the reference genome and extraction of gene hit counts, the comparison of gene expression between the defined groups of samples was performed using DESeq2.The BAM files were imported into IGV software (V2.15.2), and reads were aligned with the genome sequence of *L. pneumophila* Paris strain (NCBI accession number: NC_006368). We used IGV to visualize data as a graphical display to compare the transcriptomic data between *legK2* and *vipA* obtained from the different experiments.

2.9. Expression of Translational Fusions during Bacterial Growth in Axenic Medium or Intracellular Bacterial Growth after Infection. L. pneumophila cells expressing translational *luc*- or *gfp*-fusions were grown on BCYE agar for 24 hours at 37°C. For axenic growth, strains were inoculated at $OD_{600} = 0.04$ in 150 μL AYE medium supplemented with 0.2 mg.mL^{-1} D-luciferin (122796; Perkin Elmer). The 96-well plate was placed in microplate reader (Tecan) at 30°C or 37°C and submitted to intermittent shaking. Growth (OD_{600}) and luminescence signals were monitored every 15 min during 72 hours. For intracellular growth, infection of *A. castellanii* was performed as described above. Intracellular growth and translational *gfp*-fusion expression were monitored in a microplate reader (Tecan) by measuring mCherry fluorescence at λex = 560 nm and λem = 610 nm, and GFP fluorescence at λex = 480 nm and λem = 520 nm, respectively.

2.10. Sample Preparation and Mass Spectrometry. Three independent cultures of *L. pneumophila* Paris WT were made in liquid medium AYE at 30°C until reaching OD_{600nm} 1, 2, 3, 4, and 5. Then, a pellet of 3.10^9 bacteria was made for each independent culture and stored at -80°C for 24 hours. The cells of each pellet were then lysed by adding 200 μl of B-PER (bacterial protein extraction reagent) (ThermoScientific) followed by a 15-minute incubation at 37°C and a 30-minute centrifugation at 21 000 g at 4°C. The clear lysates were then recovered, and concentration was determined by Bradford assay using the Coomassie Plus kit (Thermo Scientific) according to the manufacturer's instructions. For each sample, 50 μg of proteins were precipitated with TCA. Pellets were washed, dried, and resolubilised in NaOH 50 mM/HEPES 1 M pH 8/H_2O-15/5/78-v/v/v, reduced with 5 mM TCEP for 45 minutes at 57°C, and then alkylated with 10 mM iodoacetamide for 30 minutes in the dark at room temperature and under agitation (850 rpm). Double digestion was performed with endoproteinase Lys-C (Wako) at a ratio of 1/100 (enzyme/proteins) in TEAB 100 mM for 5 h, followed by an overnight trypsin digestion (Promega) at a ratio 1/100 (enzyme/proteins). Both LysC and Trypsin digestions were performed at 37°C. Peptide concentration was checked before TMT labelling with quantitative fluorometric peptide assay (ThermoScientific). Each sample was labelled with TMTpro 16 plex (ThermoScientific) according to the manufacturer's instructions. This resulted in 15 samples (3 for each OD), plus one sample "pool" where all samples were mixed in equal quantity before labelling. Then, 2 μg of each of the 16 labelled samples was mixed and dried up. The pellet was resuspended in 300 μl 0,1% TFA and fractionated on a high pH reserved-phase fractionation spin-column (Thermo Scientific) according to the manufacturer's instructions for TMT-labelled peptide samples. Recovered fractions were dried up and then resuspended in 10 μl 2% ACN + 0.1% formic acid. All fractions were then analyzed in triplicate by mass spectrometry (Q Exactive HF coupled with nanoRSLC Ultimate 3000, ThermoScientific). 1 μL of each fraction was injected and loaded on a C18 Acclaim PepMap100 trap-column 300 μm ID × 5 mm, 5 μm, 100 Å, (ThermoScientific) for 3 min at 20 μL/min with 2% ACN, 0.05% TFA in H_2O and then separated on a C18 Acclaim Pepmap100 nanocolumn, 50 cm × 75 mm i.d, 2 mm, 100 Å (ThermoScientific) with a 60 minutes linear gradient from 3.2% buffer A to 40% buffer B (A: 0.1% FA in H2O, B: 0.1% FA in ACN) and then from 40 to 90% of B in 2 min, hold for 10 min and returned to the initial conditions in 1 min for 14 min. The total duration was set to 90 minutes with a flow rate of 300 nL/min, and the oven temperature was kept constant at 40°C. Labelled peptides were analyzed with TOP15 HCD method: MS data were acquired in a data-dependent strategy selecting the fragmentation events based on the 15 most abundant precursor ions in the survey scan (375-1800 Th). The resolution of the survey scan was 120,000 at m/z 200 Th and for MS/MS scan the resolution was set to 45000 at m/z 200 Th. The ion target value for the survey scans in the Orbitrap and the MS/MS scan were set to 3E6 and 1E5, respectively, and the maximum injection time was, set to 50 ms for MS scan and 100 ms for MS/MS scan. Parameters for acquiring HCD MS/MS spectra were as follows; collision energy = 32 and an isolation width of 1.2 m/z. The precursors with unknown charge state, charge state of 1 and 8 or greater than 8, were excluded. Peptides selected for MS/MS acquisition were then placed on an exclusion list for 30 s using the dynamic exclusion mode to limit duplicate spectra. Data were analyzed using Proteome Discoverer 2.4 with the SEQUEST HT search engine on the *L. pneumophila* genome from NCBI (NC_006368) and a database of common contaminants. Precursor mass tolerance was set at 10 ppm, fragment mass tolerance was set at 0.02 Da, and up to 2 missed cleavages were allowed. Oxidation (M), acetylation (protein N-terminus), and phosphorylation (S, T, and Y) were set as variable modification and TMTpro labelled peptides in primary amino groups (K and N-ter) and carbamidomethylation

(C) as fixed modification. Validation of identified peptides and proteins was done using a target decoy approach with a false positive (FDR < 1%) via percolator. Protein quantitation was performed with reporter ions quantifier node in Proteome Discoverer 2.4 software with integration tolerance of 20 ppm, peptide and protein quantitation based on pairwise ratios and t-test hypothesis test. Protein expression of RocC, VipA, and LegK2 were extracted from the obtained dataset (see Supplementary Data S8). RocC was used as a control as its expression has been extensively studied via classical methods (Western blot) [23]. LegK2 was not detected.

2.11. TEM Translocation Assays. U937 cells grown in RPMI supplemented with 10% FCS were plated in black clear-bottom 96-well plate at a 1×10^5 cells/well concentration in the presence of 100 ng/mL of Phorbol-12-myristate-13-acetate (PMA) to allow differentiation of U937 cells in macrophages. Overnight cultures of *L. pneumophila* strains carrying either pXDC61-*legK2* or pXDC61-*vipA* were grown in AYE + 5 μg/mL chloramphenicol and 500 μM IPTG to induce the production of TEM-fused proteins. Bacterial suspension in RPMI at 2×10^8 cells/mL was used to infect U937 cells (MOI = 50). After centrifugation at 2500 rpm for 10 min to initiate bacteria-cell contact, the infected cells were incubated at 37°C with 5% CO_2. At different time points, 10 μM of CCCP were added to block effector translocation through the Dot/Icm T4SS. Cell monolayers were then loaded with the fluorescent substrate by adding 20 μl of 6X CCF4/AM solution (LiveBLAzer-FRET B/G Loading Kit, Invitrogen) containing 15 mM Probenecid (Sigma). The cells were incubated for an additional 90 min at room temperature. Fluorescence was quantified on an Infinite M200 microplate reader (Tecan) with excitation at 405 nm (10 nm band-pass), and emission was detected via 460 nm (40 nm band-pass, blue fluorescence) and 530 nm (30 nm band-pass, green fluorescence) filters.

2.12. Protein Localization in Transfected Mammalian Cells. HeLa cells were plated one day before transfection on sterile glass coverslips and transfected or cotransfected with empty pDEST27 or pDEST27-*legK2,* empty peGFP or peGFP-N-VipA and/or pCI-Neo3Flag-ARPC1B using JetPrime (Polyplus). At 24 h posttransfection, cells were fixed with 4% formaldehyde, quenched with 0,1 μg/ml glycine, permeabilized with 0.3% Triton X-100, and blocked with 1% BSA. GST and GST-LegK2 proteins were labelled with an anti-GST antibody from rabbit (A7340; Sigma) and detected with an anti-rabbit secondary antibody from goat conjugated with the fluorochrome Alexa Fluor 488 (A11034; ThermoFisher Scientific) or fluorochrome Alexa Fluor 594 (A11037; ThermoFisher Scientific). Flag-ARPC1B were labelled with anti-Flag antibody from mouse (F1804; Sigma) and detected with anti-mouse secondary antibody from goat conjugated with the fluorochrome Alexa Fluor 594 (A11032; ThermoFisher Scientific). EEA1 endogenous protein was labelled with an anti-EEA1 antibody from rabbit (3288S; Cell Signalling Technology). Glass slides were then mounted on slides with Fluoromount, and microscopy was carried out using a confocal laser scanning microscope (LSM800; Zeiss).

2.13. Protein Localization in D. discoideum during Infection by L. pneumophila. D. discoideum cells were plated on sterile glass coverslips a day before infection in MB medium (7.15 g/L yeast extract; 14.3 g/L peptone; 20 mM MES and buffered at a pH 6.9) and incubated overnight at 22°C. Monolayers were infected the next day at an MOI of 50 with HA-protein -expressing bacteria grown overnight at 37°C in AYE 1X medium supplemented with chloramphenicol and IPTG for maintenance and induction of HA expression plasmid. Plates were then spun at 2000 rpm for 10 min and incubated at 25°C. At different time points, monolayers were fixed with 4% formaldehyde, permeabilized with 0.1% Triton X-100 for 5 min at RT, and blocked in 0.2% BSA for 1 h at RT. HA-fusion proteins were stained with anti-HA primary antibodies (3724, Cell Signaling Technology) and then with anti-rabbit-coupled to Alexa Fluor 594 antibodies (A-11037; ThermoFisher Scientific). Glass slides were then mounted on slides with Fluoromount+DAPI (Thermoscientific), and microscopy was carried out using a confocal laser scanning microscope (LSM800; Zeiss).

2.14. Coimmunoprecipitation by GFP-Trap. HeLa cells were plated in a 10 cm Petri dish the day before transfection in DMEM supplemented with 10% fetal calf serum FCS. The next day, they were cotransfected with either pDEST27 or pDEST27-*legK2*, empty peGFP, peGFP-C-VipA, or peGFP-N-VipA using JetPrime (Polyplus). At 24 h posttransfection, cells were harvested in ice-cold PBS, washed and pelleted cells were lysed during 1 h in ice-cold RIPA buffer (10 mM Tris, pH 7.5, 150 mM NaCl, 0.5 mM EDTA, 0.1% SDS,1% Triton X100, 1% deoxycholate, benzonaze, 2,5 mM $MgCl_2$, 1 mM PMSF and protease inhibitors) at 4°C with gentle agitation. Lysed extracts were then centrifuged at 20 000 g for 10 min at 4°C. Lysates were diluted in washing buffer and then incubated with washed GFP-Trap® Agarose beads (Chromotek) for 1 h30. After incubation, beads were collected by centrifugation and washed three times before eluting GFP-tagged proteins and their potential interactants in 100 μL of Laemmli buffer 2X at 95°C for 7 min.

2.15. In Vitro Phosphorylation Assays. E. coli BL21 (DE3) strains carrying either pGEX-*legK2* or pQE30-*vipA* were grown at 37°C until cultures reached an OD_{600} of 0.7. Then, IPTG was added to a final concentration of 0.2 mM, and growth was continued overnight at 20°C. Pellets were resuspended in GST-pull down equilibration/wash buffer (125 mM Tris-HCl pH 7.5, 150 mM NaCl+protease inhibitor cocktail (Sigma)+1 mg/ml lysozyme) or in 6His-pull down equilibration/wash buffer (50 mM Tris-HCl pH 7.5, 150 mM NaCl and 10 mM imidazole+protease inhibitor cocktail (Sigma)+1 mg/ml lysozyme), and bacteria were lysed using 3 passages in a French Press (SLM, Urbana, IL). After lysate centrifugation at 12 000 g for 30 min, supernatants were collected and transferred to tubes containing either Pierce™ Gluthatione Magnetic Agarose Beads (ThermoFisher Scientific) or TALON Metal Affinity Resin

(Takara Bio), respectively, according to the manufacturers' recommendations. The purity of the eluted protein was analyzed by SDS-PAGE. *In vitro* phosphorylation of 2 μg of purified 6His-VipA fusion protein was performed for 30 min at 37°C in 20 μl of a buffer containing 25 mM Tris-HCl pH 7.5, 5 mM MnCl2, 5 mM dithiothreitol, 100 mM ATP. 1 μg of myelin basic protein (MBP) was added as positive phosphorylation control for LegK2. In each case, the reaction was stopped by the addition of an equal volume of 2X Laemmli loading buffer. Proteins were then separated by SDS-PAGE and immunoblotted with an anti-phosphothreonine monoclonal antibody (CST; #9381).

2.16. Phylogenetic Profiles of VipA and LegK2. A total of 647 annotated *Legionella* sp. and *Coxiella burnetii* genomes were downloaded from NCBI as of October 2017 (accession numbers are available in Supplementary Data S4). We used MMSEQS2 (default parameters) [24] to cluster the annotated proteins into families. 95 universal-unicopy families were aligned with MAFFT (default parameters) [25] and concatenated at the nucleotide level to reconstruct a phylogenetic tree using FastTree2.1 [26]. We used Treemmer [27] to select 120 genomes representing the phylogenetic diversity in this tree, with the constraint that the 19 *L. pneumophila* genomes missing either VipA or LegK2 were represented. This tree was then used in count [28], with the complete table of presence/absence of proteins in the corresponding genomes to infer the parameters of the probabilistic model of gain-duplication-loss. These parameters were then used to reconstruct the ancestral presence/absence of all genes. We finally used iTOL [29] to represent the evolutionary history of VipA and LegK2.

3. Results

3.1. LegK2/VipA Effector Pair Controls Actin Polymerization at the Surface of the LCV. Taking into account the antagonistic activities of LegK2 and VipA towards actin polymerization and the localization and role of LegK2 in the inhibition of actin polymerization on the LCV, we hypothesized that LegK2/VipA may cooperatively contribute to the remodeling of actin cytoskeleton at the surface of the LCV during *Legionella* infection.

Scar-free single mutants *ΔlegK2*, *ΔvipA*, and double mutant *ΔlegK2*/*ΔvipA* of *L. pneumophila* Paris strain were constructed in two steps, taking advantage of a homologous-recombination strategy with the counter-selectable *mazF-kan* cassette, as previously described [21]. *Dictyostelium discoideum* was infected with mCherry-producing *L. pneumophila* Paris strain, *ΔdotA*, *ΔlegK2*, *ΔvipA* single mutants, or *ΔlegK2*/*ΔvipA* double-mutant strains, and polymerized actin was visualized with phalloidin-FITC, 15 min postinfection (Figure 1(a)). While less than 5% of WT bacterium-containing vacuoles were labelled with phalloidin, more than 20% of the avirulent *dotA* mutant-containing vacuoles were actin-positive (Figure 1(b)). This significative difference highlights the importance of local actin remodeling on the LCV during *Legionella* infectious cycle. Indeed, less than 1 min after engulfment of the bacteria, cortical actin associated with the bacterial entry sites during phagocytosis dissociates from the LCV [30]. Similarly to what was reported for the Lens strain [16], 18% of *ΔlegK2* Paris mutant LCVs were labelled with phalloidin, thus confirming that LegK2 plays a key role in the inhibition of actin polymerization at the surface of the LCV (Figure 1(b)). In contrast, the contribution of VipA in controlling actin polymerization on the LCV surface is limited or nondetectable, as only 3.5% of LCVs are decorated with polymerized actin in the *ΔvipA* mutant, which is not significantly different from the parental Paris strain. Nevertheless, this activity is able to compensate for the actin polymerization inhibition defect caused by the absence of LegK2, as 5% of the vacuoles containing the *ΔlegK2*/*ΔvipA* double mutant are actin-positive, which is not significantly different from the parental strain but significantly different to that observed in the *ΔlegK2* mutant (Figure 1(b)).

Taken together, these data point out that deletion of *vipA* restores the *ΔlegK2* mutant defect in controlling actin polymerization at the surface of the LCV, thus demonstrating that the LegK2/VipA effector pair cooperatively controls actin polymerization during the early stages of *L. pneumophila* infection.

3.2. Deletion of VipA Suppresses the Endosomal Escape and Intracellular Replication Defects of the ΔlegK2 Mutant. In addition to sharing antagonistic activities towards actin polymerization, both LegK2 and VipA target the host cell endosomal pathway. Specifically, LegK2 has been shown to inhibit actin polymerization at the LCV surface and subsequent recruitment of late endosomes/lysosomes to the vacuole surface [16], and VipA is an actin nucleator that colocalizes with early endosomes and has been proposed to disrupt normal vacuolar trafficking pathways in host cells [14]. In this context, we addressed the question of the functional relationship between these two effectors regarding phagosome maturation, in particular their contribution to the inhibition of LCV fusion with late endosomes. *D. discoideum* was infected with mCherry labelled *L. pneumophila* Paris strain WT, *ΔdotA*, single *ΔlegK2*- or *ΔvipA* mutants, or the double *ΔlegK2*/*ΔvipA* mutant, and the late endosomal or lysosomal vacuolar H^+-ATPase (V-ATPase) was labelled 1 h postinfection by immunofluorescence with anti-VatA antibodies (Figure 2(a)). As expected, the *ΔdotA* mutant is unable to block phagosome maturation and shows much more VatA-positive vacuoles (38%) compared to a WT strain (12.8%) (Figure 2(b)). Reminiscent to the *ΔdotA* strain, the *ΔlegK2* mutant presents about 36% of VatA-positive vacuoles, which confirms that LegK2 plays a key role in the inhibition of phagosome maturation (Figure 2(b)). Interestingly, while only 13% of vacuoles were VatA-positive for the *ΔvipA* strain (which indicates that VipA is not necessary to inhibit phagosome maturation), the *ΔlegK2*/*ΔvipA* double-mutant also shows 12% of VatA-positive vacuoles which is not significantly different from the WT-containing vacuoles (Figure 2(b)). Thus, the *ΔvipA* mutation is able to compensate for the phagosome maturation defect caused by the *ΔlegK2* mutation.

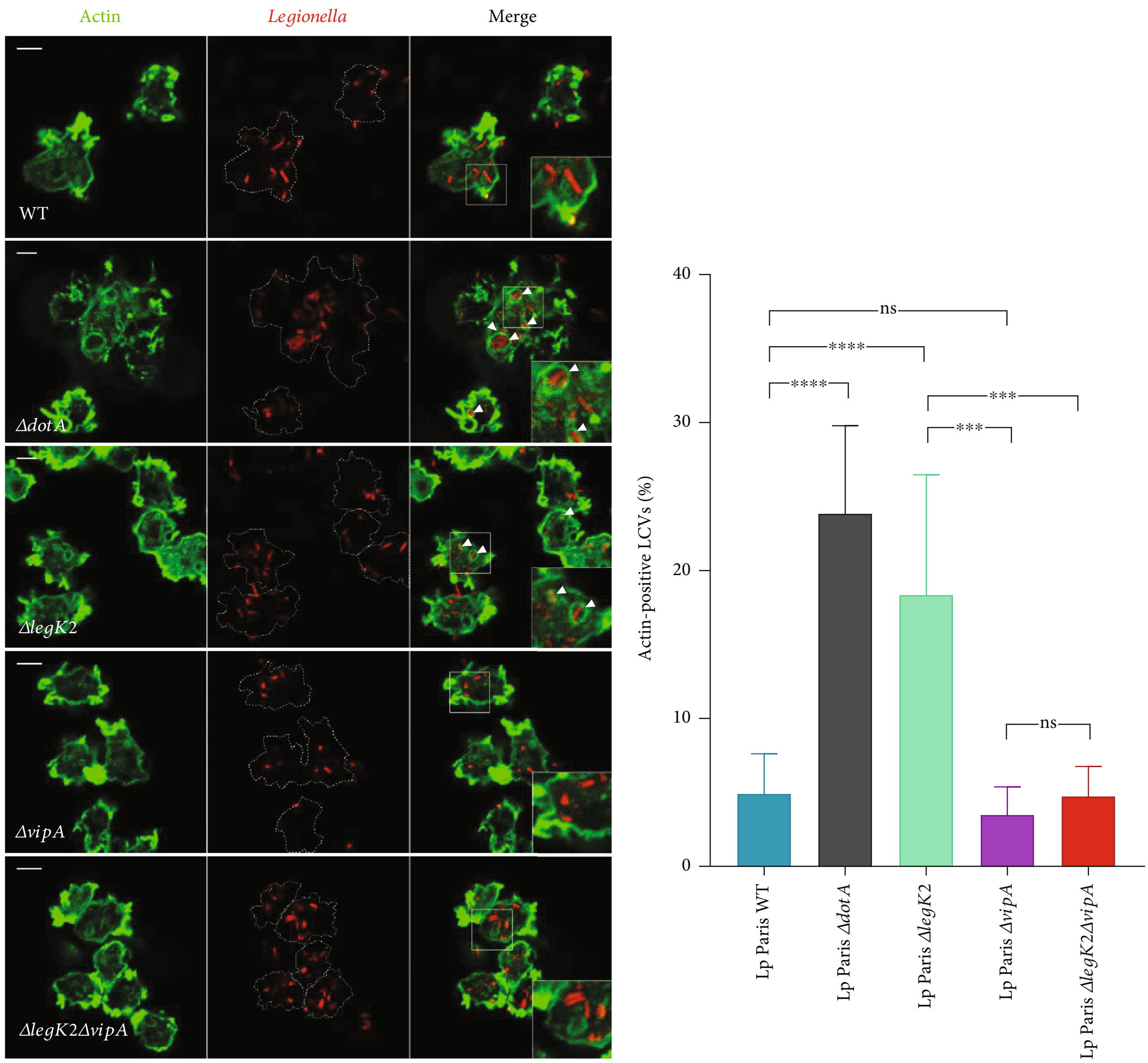

(a) (b)

Figure 1: LegK2/VipA effector pair controls actin polymerization at the surface of the LCV. (a) Actin polymerization on LCVs during *Legionella* infection. *D. discoideum* was infected for 15 min at an MOI of 100 with mCherry-labelled WT, *ΔdotA*-, *ΔlegK2*-, *ΔvipA*-, and *ΔlegK2*/*ΔvipA*- mutant *L. pneumophila* strains. Polymerized actin on LCVs was detected by labelling with phalloidin-FITC. White arrows show examples of actin-positive LCVs. Scale bar, 10 μm. (b) Detection of polymerized actin in *ΔdotA*, *ΔlegK2*, *ΔvipA*, and *ΔlegK2*/*ΔvipA* mutant-containing vacuoles. Actin-positive vacuoles ($n > 100$) were counted for amoeba infected with *L. pneumophila* WT, the derivative *ΔdotA*, *ΔlegK2*, *ΔvipA*, and *ΔlegK2*/*ΔvipA* mutants. Quantification data are representative of three independent experiments, and the error bars represent the standard deviations from triplicates. Statistical analyses were performed using one-way ANOVA test. ns: no significant difference; $^{*}p < 0.05$; $^{**}p < 0.005$; $^{***}p < 0.0005$; $^{****}p < 0.0001$.

The ability of *L. pneumophila* to escape endosomal degradation is the prerequisite for its intracellular replication. Therefore, we sought to identify whether the LegK2/VipA functional interaction could impact *L. pneumophila* intracellular replication. *L. pneumophila* Paris strain or its mutant derivatives expressing the mCherry fluorescent protein on a plasmid were used to infect the amoeba *Acanthamoeba castellanii* at a MOI of 5. Bacterial intracellular growth was monitored by fluorescence measurement during 84 h (Figure 2(c)). As expected, WT *L. pneumophila* started efficient intracellular growth at 40 h postinfection, while the T4SS *ΔdotA* mutant failed to replicate. The *ΔvipA* mutant showed intracellular multiplication from the same time with the same growth rate compared to the Paris strain, while the *ΔlegK2* mutant was significantly delayed for intracellular multiplication, as previously reported for Lens strain [31], thus confirming the key role of this effector in the virulence of *L. pneumophila*. More interestingly, the deletion of *vipA* fully

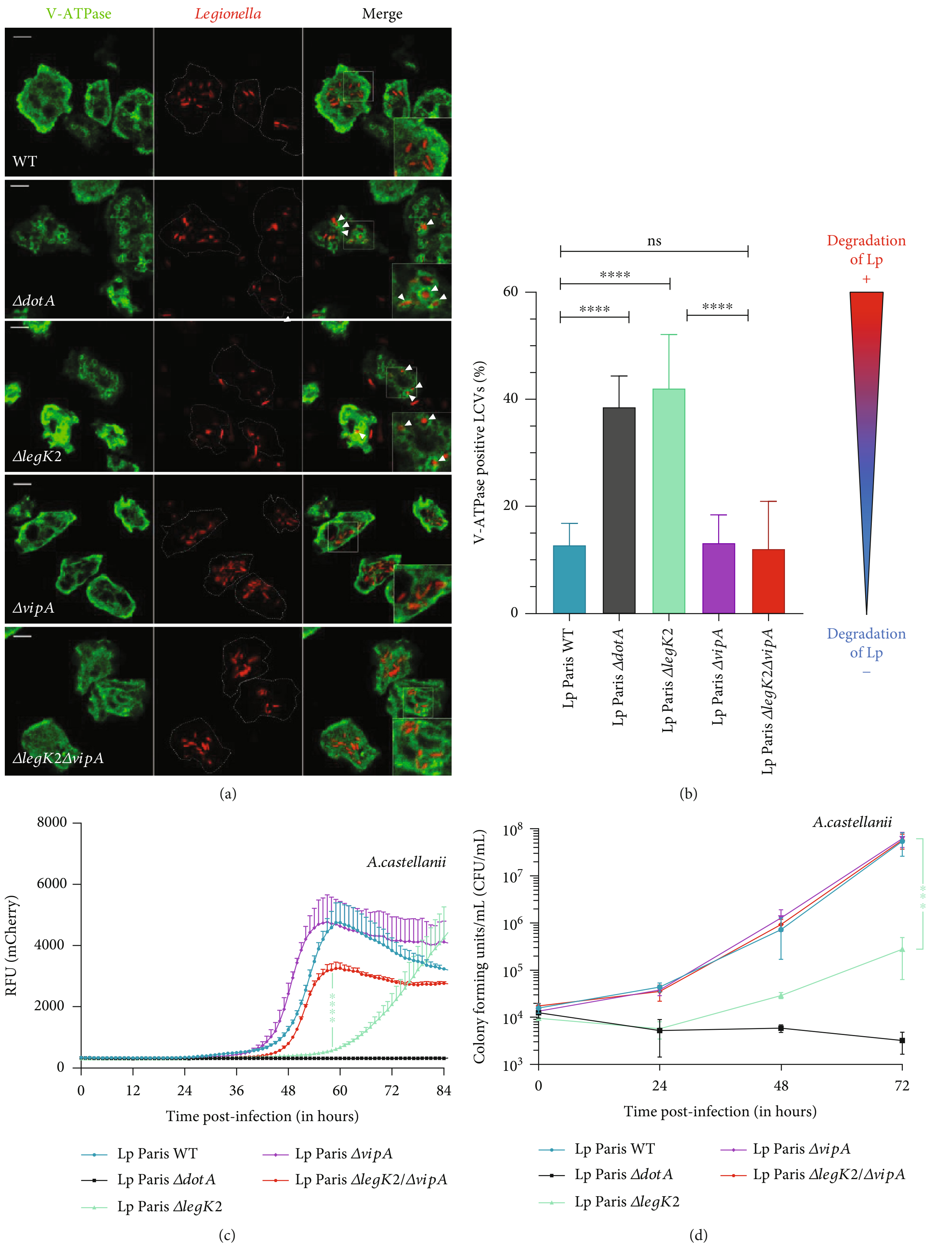

Figure 2: Continued.

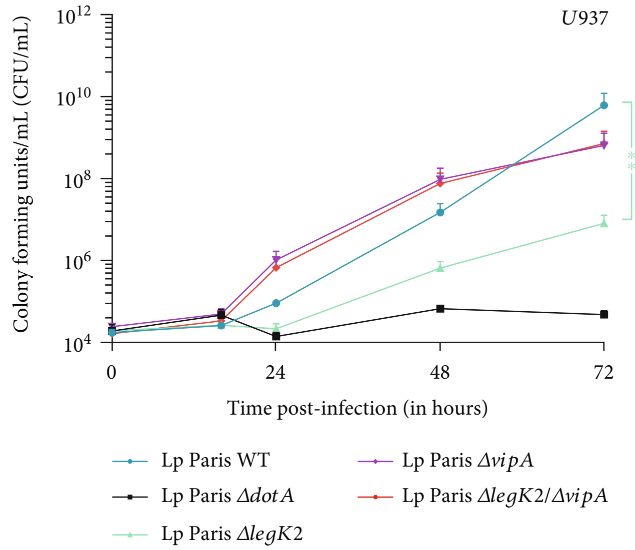

(e)

Figure 2: Deletion of *vipA* suppresses the endosomal escape and intracellular replication defects of the *ΔlegK2* mutant. (a) Acquisition of vacuolar proton ATPase on LCVs. *D. discoideum* was infected for 1 h at an MOI of 100 with mCherry-labelled WT, *ΔdotA*, *ΔlegK2*, *ΔvipA*, and *ΔlegK2*/*ΔvipA* mutant *L. pneumophila* strains. The presence of vacuolar V-ATPase on LCVs was detected by an immunofluorescence assay with anti-VatA antibodies. (b) Detection of V-ATPase on LCVs containing *L. pneumophila* Paris WT strain, Δ*dotA*, Δ*legK2*, Δ*vipA*, and Δ*legK2*/Δ*vipA* *L. pneumophila* mutants. VatA-positive vacuoles ($n > 100$) in amoebae infected with *L. pneumophila* WT, the derivative Δ*dotA*, Δ*legK2*, Δ*vipA*, and Δ*legK2*/Δ*vipA*, mutants were counted. (c) Intracellular replication of *L. pneumophila* in *A. castellanii* measured by fluorescence. *A. castellanii* amoebae were infected at MOI = 5 with *L. pneumophila* Paris WT strain or *ΔdotA*, *ΔlegK2*, *ΔvipA*, and *ΔlegK2*/*ΔvipA* mutant *L. pneumophila* strains transformed with mCherry-expressing plasmids, and intracellular replication was monitored by quantifying mCherry-fluorescence intensity. (d, e) Intracellular replication of *L. pneumophila* in *A. castellanii* (d) and in U937-derived macrophages (e), measured by CFU. *A. castellanii* amoebae and U937-derived macrophages were infected at MOI = 5 and MOI = 1, respectively, with *L. pneumophila* Paris WT strain, Δ*dotA*, Δ*legK2*, Δ*vipA*, and Δ*legK2*/Δ*vipA* mutant *L. pneumophila* strains, and intracellular replication was monitored by numbering CFU (colony forming units) after amoeba/macrophages lysis at different times postinfection on BCYE agar medium. (b–e) The results shown are representative of three independent experiments, and the error bars represent the standard deviations from triplicates. Statistical analyses were performed using a one-way ANOVA test for V-ATPase detection on LCVs and a two-way ANOVA test for intracellular replication: ns, no significant difference; $^{*}p < 0.05$; $^{**}p < 0.005$; $^{***}p < 0.0005$; $^{****}p < 0.0001$.

complements the intracellular multiplication defect of the *ΔlegK2* mutant, revealing the first example of effector-effector functional interaction with strong impact on *L. pneumophila* virulence (Figure 2(c)). The functional complementation of *ΔlegK2* mutant by the *ΔvipA* deletion was confirmed by numbering the CFU resulting from the lysis of *A. castellanii* infected by *ΔlegK2*, *ΔvipA*, or double mutant *ΔlegK2*/*ΔvipA* strains (Figure 2(d)). The same phenotype was observed upon infection of U937 macrophages (Figure 2(e)). Importantly, full genome sequencing of *ΔlegK2*, *ΔvipA*, and *Δ*legK2/*ΔvipA* strains revealed no other secondary mutations, confirming that the complementation of the intracellular replication defect of *ΔlegK2* strain is solely due to the deletion of the *vipA* gene (Supplementary Data S5). It is noteworthy that none of the single and double mutants shows an axenic growth defect (Supplementary Data S6).

Together, these data identify the first effector-effector suppression pair targeting the host cell actin cytoskeleton and show that LegK2/VipA pair contributes to bacterial escape from the endosomal pathway and its subsequent intracellular replication. They also suggest that VipA contributes to the direct or nondirect control of LCV/endosome interaction, consistent with its localization with early endosomes in transfected cells, thus revealing its role in the *L. pneumophila* infectious cycle, despite the absence of a defect of the single *vipA* deleted mutant.

3.3. LegK2 and VipA Effectors Are Produced and Secreted at the Early Stage of Infection. To investigate in detail the molecular relationship between LegK2 and VipA effectors, we addressed their expression/secretion pattern. First, we performed an RNA-seq from *L. pneumophila* Paris strain grown at 37°C in nutrient-rich medium to exponential (expo; OD_{600} 1.5), postexponential (postexpo; OD_{600} 4 and visual check of motility acquisition), and to the onset of stationary (Stat; OD_{600}~6) growth phase. Read counts mapped on *L. pneumophila* Paris genome show that both *vipA* and *legK2* genes are weakly expressed, when compared with the 2000 reads of *ravK* that encodes another host actin targeting effector. Nevertheless, while *vipA* mRNA is expressed in the exponential growth phase compared to the other two phases (Figure 3(a)), *legK2* mRNA reads are mostly detected in postexponential and stationary phases (Figure 3(b)). These results are in accordance with other RNAseq analysis available in the literature and realized by Sahr et al. [32]. In addition, we constructed chromosomal translational fusions of

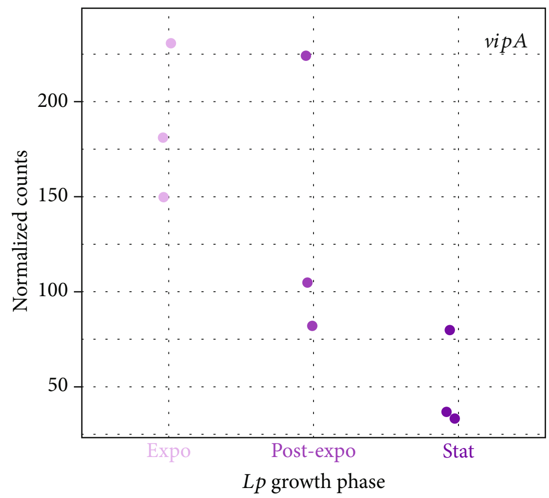

(a)

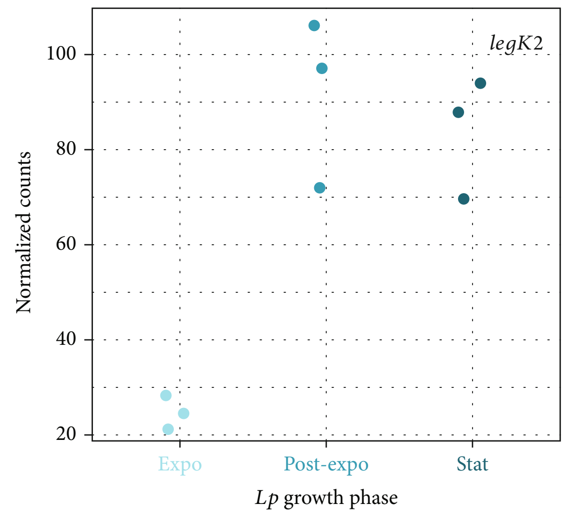

(b)

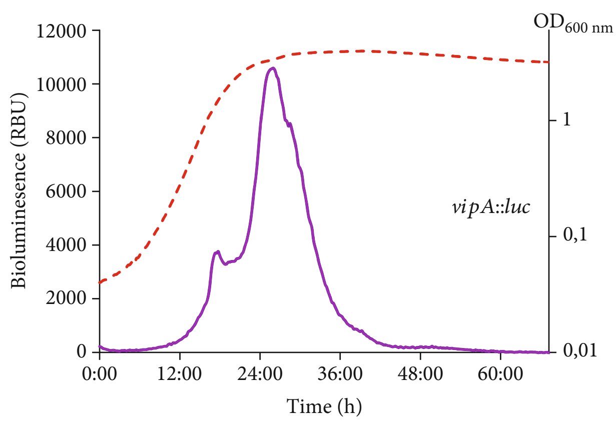

(c)

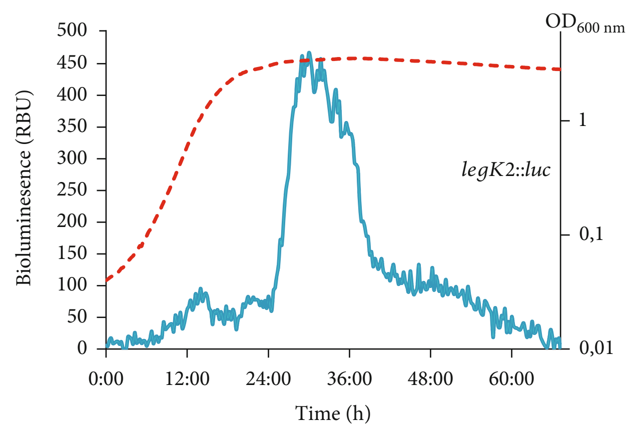

(d)

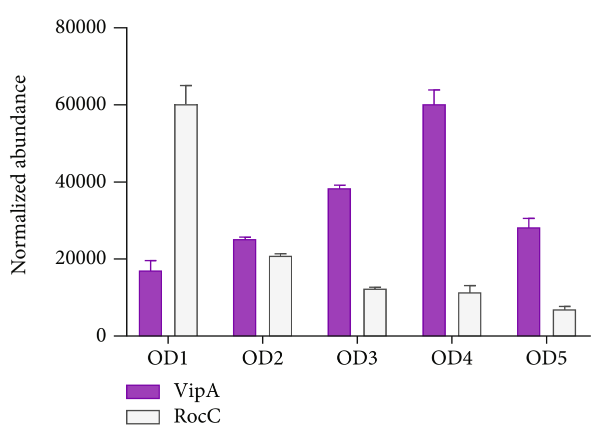

Mean normalized abundance

		OD1	OD2	OD3	OD4	OD5
LegK2		ND	ND	ND	ND	ND
VipA	Mean	16921	25058	38261	60027	28108
	SD	2706	735	1002	3905	2519
RocC	Mean	60251	20693	12173	11246	7058
	SD	4833	715	581	1908	832

(e)

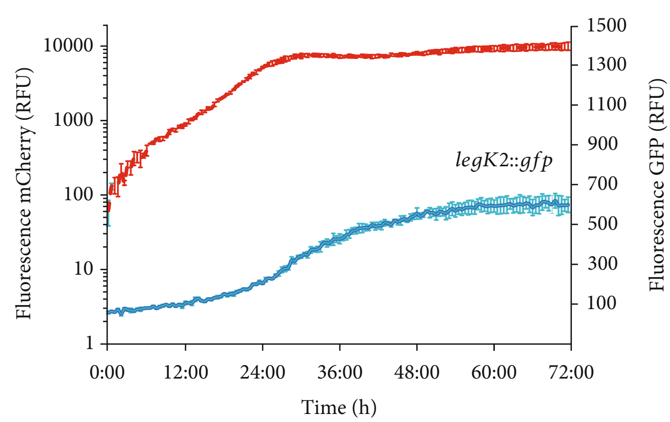

(f)

Figure 3: Continued.

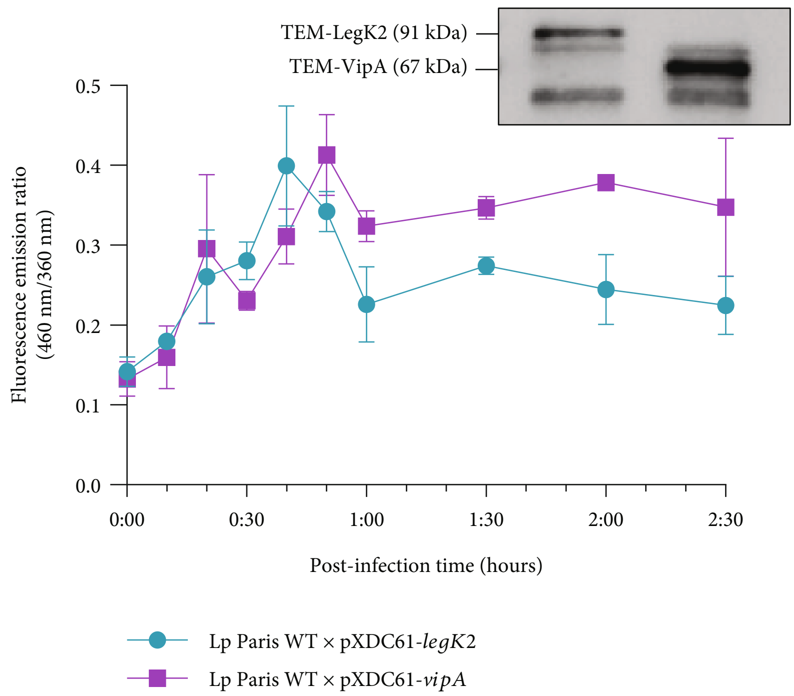

(g)

Figure 3: LegK2 and VipA effectors are produced and secreted at the early stage of infection. *legK2* and *vipA* genes are weakly expressed, mostly in the exponential growth phase for *vipA* (a) and in postexponential and stationary phases for *legK2* (b). Three cultures of *L. pneumophila* Paris WT were grown in liquid medium AYE (37°C). At the desired growth phases (exponential/OD_{600} = 1.5, postexponential/start of mobility acquisition /OD600 = 4, and stationary collected 2 hours after the postexponential sample), samples were collected, and their RNA content was analyzed by RNAseq. The graphs show normalized read counts of *legK2* or *vipA* mRNAs for each sample at the different growth phases. (c, d) Production of VipA-Luc and LegK2-Luc fusion proteins is maximum at the onset of the stationary growth phase. Luminescence emission from chromosomal translational fusions of *vipA::luc* (c) and *legK2::luc* (d) in *L. pneumophila* Paris strain grown in AYE medium at 37°C measured by OD_{600} (dashed red lines). The data shown are representative of 3 independent clones of each fusion. (e) VipA accumulates in *L. pneumophila* up to D O_{600} = 4. Three independent cultures of *L. pneumophila* Paris WT were grown in liquid medium AYE (at 30°C). At the desired OD_{600} (1–5), samples were collected, and their protein content was analyzed by mass spectrometry after sample-specific labelling (see Materials and Methods for details). The graphs show the normalized abundance of protein detected at each OD_{600}. The LegK2 protein has not been detected in our conditions. The RocC protein is used as a control as it is detected at the same range of quantity as VipA, and its production during growth was previously studied by Western blot [23]. Of note, the RocC pattern of production detected by mass spectrometry corresponds to the one previously obtained by Western blot [23]. (f) *legK2* is expressed during *A. castellanii* infection at the onset of the transmissive phase. A chromosomal *legK2::gfp* translational fusion was constructed in a mCherry expressing Paris strain. After infection of *A. castellanii* amoebae, the mCherry fluorescence was used to monitor the bacteria intracellular multiplication (dashed red line), and the GFP fluorescence was a read out of the *legK2* gene expression (blue line). The data shown are representative of 3 independent clones of each fusion. (g) Translocation kinetics of TEM-LegK2 and TEM-VipA fusion proteins. U937 cells were infected (MOI = 20) with wild-type (WT) Paris strains expressing plasmidic TEM-fusion proteins, TEM-LegK2 or TEM-VipA. Induction of fusion protein expression by 0.5 mM IPTG has been monitored by Western blot analysis. Results are obtained from 3 independent experiments made in triplicates and are presented as means ± SD.

vipA::luc and *legK2::luc* encoding VipA- and LegK2-luciferase fusions, respectively, introduced these fusions at the original site of the *vipA* and *legK2* genes on the chromosome of *L. pneumophila* Paris strain, and monitored the luminescence produced by bacteria grown in AYE medium at 37°C. Luminescence emission reveals that production of the fusion proteins VipA-Luc and LegK2-Luc is strongly controlled, with maximum production at the onset of the stationary growth phase, more precisely VipA-Luc (Figure 3(c)) slightly ahead of LegK2-Luc (Figure 3(d)). Importantly, the luminescence intensity generated by the VipA-Luc fusion is 25 times greater than that produced by the LegK2-Luc fusion, suggesting that *vipA* is more highly expressed than *legK2*. The timing and level of VipA-Luc and LegK2-Luc protein fusions are the same when bacteria are grown at 30°C, indicating that *vipA* and *legK2* gene expression is not dependent on growth temperature (supplementary data S7). To confirm the translational fusion data, the relative amount of *L. pneumophila* Paris WT proteome at different OD during growth in nutrient-rich medium was analyzed, by a high-resolution quantitative mass spectrometry approach (Figure 3(e)). Of note, the RocC protein used as a control was detected by this approach according to a pattern similar to the one previously obtained by Western blot [23]. VipA was detected accumulating from OD_{600} = 1 to OD_{600} = 4 before diminishing at OD_{600} = 5 (Figure 3(e); Supplementary Data S8). As the RNAseq data showed that the gene was more expressed during the exponential phase, these mass spectrometry data, consistent with the translational fusions data, suggest an unreported posttranscriptional control that results in the main production of VipA during the postexponential growth phase. Consistent with the low level of LegK2-Luc luminescence, the LegK2 protein was not detected by mass spectrometry at any growth phase, confirming its low expression level. To ensure that *legK2* is expressed during infection, despite its low level of expression in axenic medium, a chromosomal *legK2::gfp* translational fusion was constructed in *L. pneumophila* Paris strain expressing *legK2* cloned on pXDC50 (to complement the chromosomic *legK2* copy which encodes a nonsecreted LegK2-GFP protein). After infection of *A. castellanii* amoebae, the mCherry fluorescence from pXDC50 was used to monitor the bacteria intracellular multiplication, and the GFP fluorescence was a read out of the chromosomic *legK2* gene expression (Figure 3(f)). Accumulation of GFP fluorescence from *legK2::gfp* fusion was observed at the onset of the stationary phase, also called the transmissive phase in infection, thus demonstrating that *legK2* is expressed during amoeba infection, with the same profile than in bacteria grown in axenic medium. Together, these data suggest that the LegK2 and VipA effectors are produced in the transmissive phase of the *Legionella* infectious cycle and, therefore, are available for secretion right after the contact with the host cell, at the early stage of the infection cycle.

Thus, we sought to establish the Dot/Icm translocation kinetics of each effector (independent of its production) by performing VipA and LegK2 kinetic translocation assays using the β-lactamase translocation reporter system [33, 34]. β-Lactamase assays were performed with plasmidic TEM-effector fusions under inducible IPTG promoter in order to (i) circumvent the low level of *legK2* and *vipA* gene expression and to (ii) decouple the two levels of control that affect the temporality of effector secretion, i.e., the expression of the effector encoding gene and the secretion itself of the effector protein. U937-derived phagocytes were infected with *L. pneumophila* strains expressing a fusion protein between the TEM-1 β-lactamase and the effector of interest (TEM-LegK2 or TEM-VipA) from a plasmidic IPTG-inducible (Ptac) promoter, as confirmed by Western blot (Figure 3(g)). At different times postinfection, secretion was inhibited by the protonophore CCCP, and levels of secreted effector were quantified by adding CCF4 to the infected cells [35]. CCF4 is composed of coumarin ($\lambda_{ex} = 409$ nm), and fluorescein linked by a β-lactam ring and fluoresces in green (520 nm). The secretion of the fusion protein TEM-effector cleaves the β-lactam ring and induces emission wavelength to change from green to blue (447 nm); measuring the blue/green ratio thus reveals the level of the secreted effector. Translocated LegK2 effector increases steadily up to 45 minutes postinfection and then decreases and stabilizes (Figure 3(g)). Reminiscent of the secretion profile obtained for LegK2, VipA levels also showed an increase up to 50 minutes postinfection (with a small intermediate peak at 20 minutes postinfection) and then a decrease and a stabilization (Figure 3(g)). Together, these data may indicate that LegK2 and VipA effectors are secreted at the same time during the early stage of *L. pneumophila* infection cycle. Noteworthy, the low level of expression of LegK2 does not prejudge the importance of its role during the infectious cycle, since its deletion strongly impairs intracellular replication of *L. pneumophila*.

3.4. The LegK2/VipA Suppression Pair Does Not Meet the Definition of Metaeffector. Effector-effector suppression is the hallmark of an emerging class of proteins called metaeffectors, or "effectors of effectors". The concept of metaeffector, even if remaining flexible, implies a direct physical interaction between an effector and its cognate effector [19]. Taking into account that LegK2 and VipA may be secreted at the same time into the host cell, we studied their localization and possible physical interaction inside eukaryotic cells. Vectors pDEST27-*legK2* and peGFP-N-*vipA* were constructed to express in mammalian cells, N-terminal GST-tagged LegK2 (GST-LegK2) and C-terminal GFP-tagged VipA (VipA-GFP), respectively. Subcellular localization of GST-LegK2 and VipA-GFP subunits was analyzed after transfection in HeLa cells. ARP2/3 complex and early endosomes were immunolabelled with anti-ArpC1B subunit and anti-EEA1 antibodies, respectively. GST-LegK2 and ArpC1b were detected in the cytoplasm and at the periphery of cells with similar staining patterns, thus suggesting that LegK2 from Paris strain colocalizes with ARPC1B (Figure 4(a)). VipA-GFP and EEA1 appeared as puncta that seem to colocalize as reported by Bugalhão et al. [36] (Figure 4(a)). Importantly, cotransfection of HeLa cells by p-DEST27-*legk2* and peGFP-N-*vipA* vectors (encoding GST-LegK2 and VipA-GFP) showed the same respective cellular sublocalization to that of LegK2 and VipA when present alone in the cell, demonstrating that each effector does not interfere with the localization of the other one (Figure 4(a)). These data, similar to those previously obtained individually for each effector [14, 16, 36], refute the hypothesis of colocalization and localization interference of LegK2 and VipA effectors in transfected mammalian cells.

Nonetheless, we sought to assess the localization of these effectors during infection. *D. discoideum* expressing the specific marker of ER, namely, calnexin fused to GFP, were infected at MOI 50 by *L. pneumophila* WT or *ΔdotA* Paris strain transformed by pMMB207c-HA-*legK2* or pMMB207c-HA-*vipA*, and the tagged fused effectors produced upon induction with IPTG were detected in the host cell by anti-tag immunofluorescence at one-hour postinfection. HA-LegK2 signal colocalizes with calnexin-GFP on the LCV surface when cells were infected with the WT Paris strain (Figure 4(b)) while no signal was detected upon infection by the *ΔdotA* mutant. Conversely, HA-VipA is not detected after secretion, neither inside the host cytosol nor on the LCV, as previously described for experiments conducted up to 8 hours postinfection [14]. Yet, VipA-derived peptides were previously identified by mass spectrometry on the LCV surface 1 h postinfection from both infected *D. discoideum* and macrophages [37]. The discrepancy between the results of immunodetection and those obtained by mass spectrometry is most likely due to the difference in sensitivity of the two techniques. Noteworthy, the localization of VipA on the surface of the LCV could result from the maturation of the

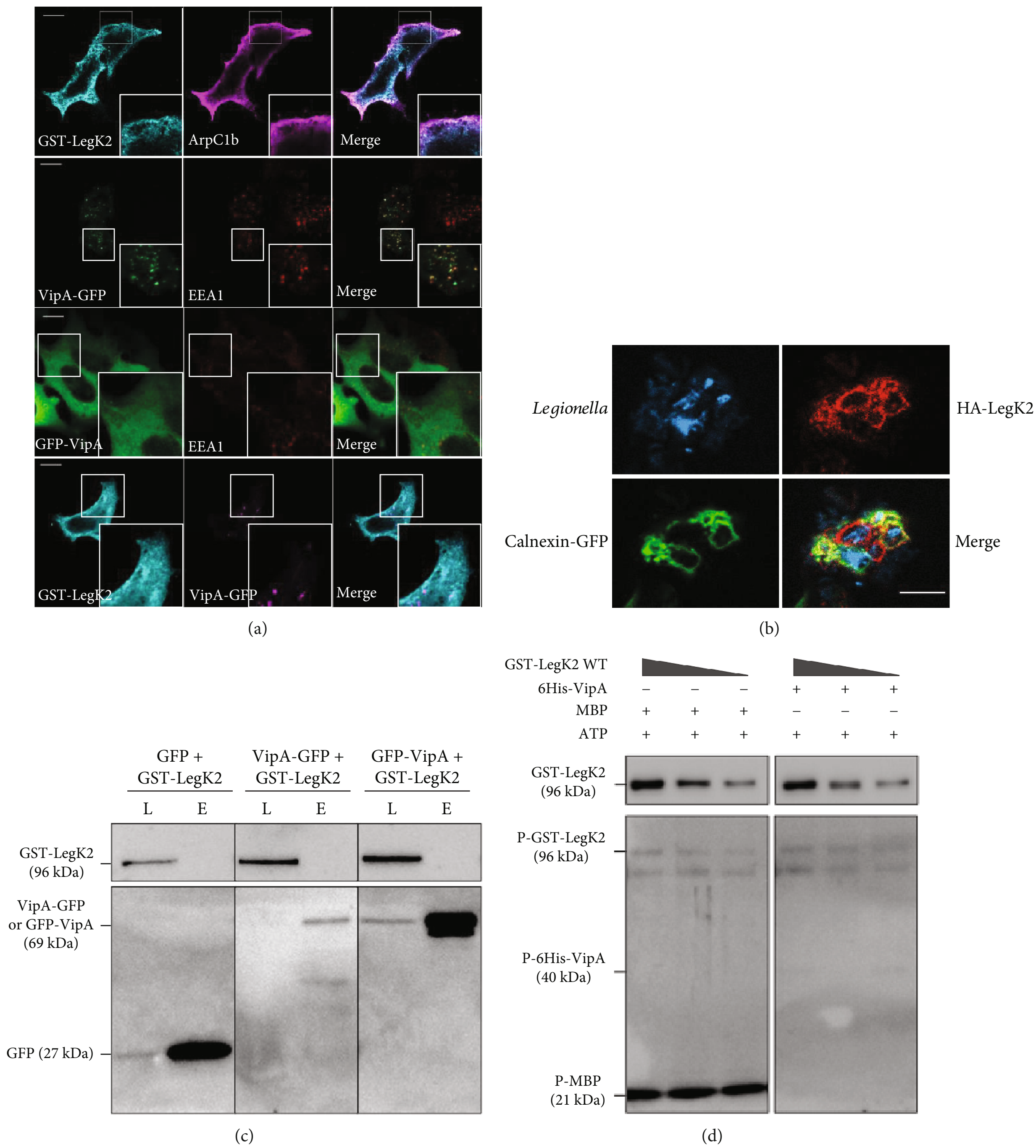

Figure 4: The LegK2/VipA suppression pair does not meet the definition of metaeffector. (a) Cellular localization of ARPC1B/LegK2 and EEA1/VipA proteins in HeLa cells transfected by pDEST27-*legK2* or peGFP-N-*vipA*. GST-LegK2 proteins were detected by immunofluorescence with anti-GST antibodies (Sigma, green), and ARPC1B was detected by anti-ARPC1B antibodies (SantaCruz; red). VipA-GFP proteins were detected thanks to GFP fusion and EEA1 by anti-EEA1 antibodies (Cell Signaling Technology). Scale bar represents 10 μm. (b) Calnexin-GFP expressing *D. discoideum* cells were infected at MOI = 50 with *L. pneumophila* WT Paris transformed with pMMB207c-Ptac-HA-*legK2* or pMMB207c-Ptac-HA-*vipA* plasmid. Infected cells were fixed 1 hour postinfection, and HA-tagged proteins were labelled by immunofluorescence with HA-antibodies. *Legionella* DNA was stained with DAPI. Scale bar represents 6 μm. (c) GFP-trap copurification assay of GFP-tagged VipA with GST-tagged LegK2 proteins. HeLa cells were cotransfected by pDEST27 or pDEST27-*legK2* and peGFP-N-*vipA* or peGFP-C-*vipA*. GFP or GFP-tagged VipA were purified on GFP-Trap agarose beads, and finally, total lysates (L) and eluted fractions (E) were immunoblotted with both anti-GST and anti-GFP antibodies. (d) *In vitro* phosphorylation assays of 6His-VipA by LegK2 detected by Western blot with antiphosphothreonine antibodies. The 6His-VipA fusion protein purified from *E. coli* BL21(DE3) was incubated with purified GST-LegK2 in the presence of 100 μM ATP. The myelin basic protein (MBP), known to be a substrate of LegK2 [31], was used as a positive control of phosphorylation. Proteins were then separated by SDS-PAGE and detected with antiphosphothreonine antibodies.

phagocytic vacuole along the endosomal pathway, which involves the fusion of the LCV with early endosomes, with which VipA colocalizes. Altogether, these data suggest that LegK2 and VipA could localize to the LCV surface during infection, at least temporarily, about 1 hour after infection.

Given this temporary common location, we investigated in mammalian cells putative interactions between GST-LegK2 and VipA-GFP by coaffinity purification. HeLa cells were cotransfected with GST-LegK2 and VipA-GFP encoding vectors, and VipA-GFP were purified by GFP-Trap. GFP-tagged VipA protein (67 kDa) was undetectable 24 h posttransfection in the soluble fraction, most likely due to its association within EEA1 membranes, but it was well purified (Figure 4(c)). Although GST-LegK2 (90 kDa) was well expressed and detected in lysates 24 h after transfection, it was not copurified with the VipA fusion protein (Figure 4(c)), suggesting that LegK2 and VipA effectors do not interact in our experimental conditions. To ensure that the low amount of VipA was not the limiting factor for detecting LegK2/VipA interaction, we sought to improve the amount of purified VipA by constructing the *peGFP-C-vipA* vector encoding the N-terminal GFP-tagged VipA (GFP-VipA). GFP-VipA that localized in the cytosol of transfected cells (Figure 4(a)) was well expressed in the soluble fraction and purified efficiently (Figure 4(c)). However, despite the high amount of GFP-VipA, GST-LegK2 was not copurified with the VipA fusion protein (Figure 4(c)). Finally, the phosphorylation status of purified 6His-VipA fusion protein was established by *in vitro* phosphorylation assays between purified proteins GST-LegK2 and 6His-VipA and analyzed by Western blot revealed with anti-phosphothreonine antibodies. Phosphorylated form of 6His-VipA protein was not detected in the presence of GST-LegK2 (Figure 4(d)). Consistently, no VipA-derivative phosphopeptides were revealed by our comprehensive proteomic analysis of *L. pneumophila* effector content, at any growth phase, thus suggesting that VipA is not a substrate of the protein kinase LegK2.

Taken together, these data demonstrate that the LegK2/VipA suppression pair does not meet the definition of metaeffector in that these effectors are not capable of interacting with each other, nor is VipA a substrate for phosphorylation of the LegK2 protein kinase. Rather, the relationship between LegK2 and VipA would be an indirect functional antagonism that occurs through counteracting activities on a shared host pathway, namely, actin polymerization at the LCV surface, by targeting two distinct cellular partners, ARP2/3 for LegK2 and G-actin for VipA.

3.5. The Functional Antagonism of LegK2/VipA Pair Is Supported by Evolutionary Cooccurrence of legK2/vipA Genes in L. pneumophila Species. The effector-effector suppression pairs are considered to have evolved to balance the targeting of host cell pathways which, if excessive, could be detrimental to the host and counterproductive for *Legionella* intracellular replication. Besides, effector/metaeffector or other effector-effector suppression pairs are often encoded by adjacent genes on the genome, presumably resulting from the simultaneous acquisition of these genes through horizontal gene transfer. Noteworthy, it is not the case for LegK2 and VipA that are encoded by distant genes on the *L. pneumophila* genome. Thus, we tested whether *legK2* and *vipA* genes have evolved independently of each other or coevolved in the genus *Legionella*. We examined the occurrences of LegK2 and VipA across 46 *Legionella* species (and *Coxiella burnetii* as an outgroup) represented by a set of 647 genomes characterized by an over-representation of *L. pneumophila* genomes (540/647) (Supplementary Data S4). Strikingly, the LegK2/VipA pair was restricted to *L. pneumophila* species, and VipA was only present in *L. pneumophila* and a clade closely related to *L. pneumophila* species, containing *L. waltersii*, *L. moravica*, *L. quateirensis*, *L. shakespearei*, and *L. worsleiensis* (Figure 5(a)). The absence of the LegK2/VipA pair in the rest of the genus *Legionella* is consistent with a previous report that showed that only 7 Dot/Icm effectors were conserved in 41 *Legionella* species, confirming the high versatility of the effector repertoire [38]. More interestingly, in *L. pneumophila*, the cooccurrence of LegK2 and VipA is highly frequent (in about 97% of the *L. pneumophila* genomes), as, among the 540 genomes of *L. pneumophila* included in our study, 6 possess only LegK2 and 11 only VipA and 1 genome have neither (Figure 5(b)). We investigated whether strains that had lost either LegK2 or VipA differed from other *L. pneumophila* strains in their conservation of other effectors known to interfere with the actin cytoskeleton. Phylogenetic study of LegK2, VipA, Ceg14, RavK, and WipA reveals that this set of effectors is conserved in *L. pneumophila* species as the five effectors are found together in 512 of the 540 *L. pneumophila* genomes (about 95%) (Figure 5(b)), and Ceg14, RavK, and WipA are conserved in the 18 strains that have lost LegK2 or VipA (Figure 5(a)). This complete set of effectors is most likely the result of an evolutionary history that selected the effector repertoire best suited to manipulate host actin polymerization to the benefit of the bacterium. Finally, we used count [28] to reconstruct the evolutionary history of the LegK2/VipA pair, onto a tree of 120 genomes representing the phylogenetic diversity of *Legionella* sp. while biasing our sample towards the 18 *L. pneumophila* genomes missing one of each gene. The analysis confirmed that VipA and LegK2 are both ancestral to *L. pneumophila* but also revealed that VipA was acquired before LegK2. VipA originated in the ancestor of a clade grouping *L. pneumophila*, *L. waltersii*, *L. moravica*, *L. quateirensis*, *L. shakespearei*, and *L. worsleiensis*, while LegK2 was specifically acquired in the ancestor of *L. pneumophila* species. Subsequently, either LegK2 or VipA were sporadically and independently lost (Supplementary S9).

4. Discussion

L. pneumophila has evolved the largest arsenal of bacterial effectors to control a sophisticated relationship with its host phagocytic cells, amoebae, or human macrophages. The record number of over 300 effectors was hypothesized to result from coevolution with its highly diverse environmental hosts to set up the best effector repertoire for each of its host. It is assumed that many effectors are needed to

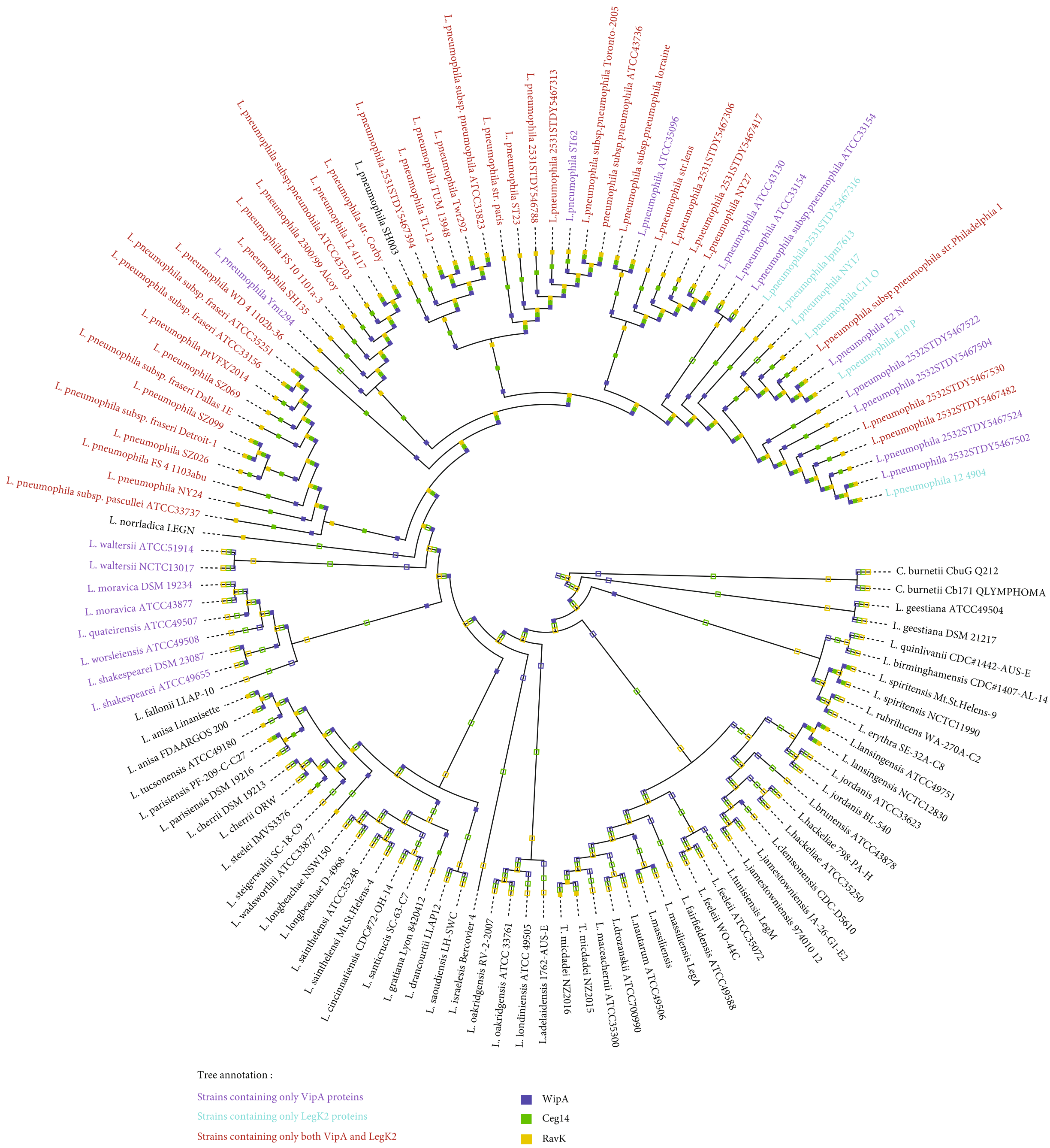

(a)

		L. pneumophila genomes	Non *L. pneumophila* genomes
	Total number of genomes	540	107
Co-occuring genes	*legK*2	528 (98%)	0
	vipA	533 (99%)	8
	*legK*2 and *vipA*	522 (97%)	0
	All 5 genes	512 (95%)	0

(b)

Figure 5: LegK2/VipA effector pair but also other actin-related effectors, Ceg14, RavK, and WipA, are strongly conserved in the *L. pneumophila* species. (a) Phylogenetic tree representing the phylogenetic diversity of *Legionella* genomes displaying either LegK2 (name of species written in blue), VipA (written in purple), Ceg14 (green squares), RavK (yellow squares), and WipA genes (dark blue). The squares are filled when the genes have been found in the corresponding genome and empty when genes have not been detected. (b) Distribution of the 5 actin-polymerization related effectors from *Legionella pneumophila* in 647 different *Legionella* strains including *L. pneumophila* and non-*pneumophila* strains. The protein sequence of the effector of *L. pneumophila* strain was blasted against our genome database of family-clustered proteins to determine the presence or absence of proteins in the corresponding genomes.

orchestrate complex and sequential interactions with numerous host cell pathways in order to support the intracellular multiplication of the bacterium. Recently, systematic screens [19, 39] or individual studies of effector function [40–48] have identified some effectors that interfere with other effector activity rather than targeting a host cell protein. Regardless of the specific activities involved in these effector-effector interactions, two main models of interaction were revealed: indirect through counteracting modification of a shared host target, such as an effector pair recently described as para-effectors that target the host cell histone H3 [49], or direct through either complex formation or the modification of one effector by another. The direct interaction model led to the emerging concept of "metaeffector".

Our study contributes to this field by identifying a novel effector-effector suppression pair, namely, LegK2/VipA, which targets the host actin cytoskeleton to support bacterial evasion from endosomal degradation and subsequent intracellular replication. This effector-effector suppression pair was not revealed by the high-throughput systematic screen based on the rescue of yeast growth defect upon heterologous expression of *L. pneumophila* effectors [19], most likely because ectopic expression of either LegK2 or VipA (yet identified to disrupt membrane trafficking in yeast [50]) does not alter yeast growth sufficiently to be detectable in the screen. Importantly, the LegK2/VipA suppression pair is physiologically relevant since it has been here identified in physiological conditions of infection of both amoeba and macrophages. We can hypothesize that the actin nucleator activity of VipA would be sufficiently cytotoxic to *Legionella* environmental and human host cells to be alleviated by the antagonistic activity of LegK2 to the benefit of the bacterium. Specifically, we demonstrated that *vipA* gene deletion rescues the *ΔlegK2* defects of inhibition of phagosome maturation along the endosomal pathway and bacterial intracellular multiplication. LegK2 and VipA antagonistic activities towards actin polymerization, i.e., inhibition of actin nucleation by LegK2 through the targeting of Arp2/3 complex versus direct actin nucleation by VipA, result in controlling actin polymerization on the LCV. In addition to the identification of the novel LegK2/VipA suppression pair, our data propose for the first time a role for VipA in the infectious cycle of *L. pneumophila*; thus, identification of effector-effector suppression pairs could be effective in circumventing the significant functional redundancy of effectors and in gaining insights into the unknown function of many Dot/Icm effectors.

The functional interaction between LegK2 and VipA is consolidated by the evolutionary biology of this pair of effectors. Indeed, both effectors are restricted to *L. pneumophila* species and are found together at a frequency of 97% in the different strains of *L. pneumophila*. VipA was acquired by the clade containing *L. pneumophila,* but also *L. waltersii*, *L. moravica*, *L. quateirensis*, *L. shakespearei*, and *L. worsleiensis* before LegK2 was specifically acquired by the *L. pneumophila* species. Then, some independent events of loss of each gene occurred very sporadically among the *L. pneumophila* phylogeny. Noteworthy, the reductive model of laboratory infection assays involving a very small number of amoeba species (usually *A. castellanii*), thereby reducing the environmental host diversity of *L. pneumophila*, does not allow for an assessment of the impact of these loss events on the intracellular replication of these *L. pneumophila* strains. Overall, the evolutionary history of LegK2/VipA pair excludes the initial model of the acquisition of effector-effector suppression pairs through a common horizontal gene transfer. It is consistent with the distant localization of *legK2* and *vipA* genes on the *L. pneumophila* genome, and likely similar for some other effector-effector suppression pairs encoded by distant genes [19].

LegK2 and VipA are likely expressed and secreted at the same time into the host cell, specifically in the transmissive phase of the *L. pneumophila* infection cycle, and they would be available to interfere with the host cell pathway at the early stage of the infection. As Urbanus et al. suggest, transcriptomics is not sufficient to place effector-effector interaction in the context of infection, and detailed proteomic analyses and secretion assays that would reveal potential controls of translation, secretion, and localization of the effectors in the cell are the next step in the field [19]. Indeed, while the *vipA* gene is more expressed in the exponential phase, the VipA protein appears to accumulate in the bacterium in the postexponential growth phase. Despite their patterns of coexpression and cosecretion, the LegK2/VipA suppression pair does not meet the definition of metaeffector. They do not seem to physically interact or colocalize inside the eukaryotic cells. Moreover, despite the fact that some metaeffectors have already been shown to target both host cell proteins and other bacterial effectors [19, 51], VipA is not a phosphorylation substrate of the protein kinase LegK2. Thus, our data on the LegK2/VipA suppression pair provide an additional model of effector-effector suppression interaction in which two effectors with antagonistic activities towards distinct actors of the same host cell pathway finely cooperate to modulate the host cell to the benefit of the bacterium. Given that LegK2 is detected on the LCV surface 1 h postinfection [16] and that VipA-derived peptides were identified at the LCV 1 h postinfection [37], it can be hypothesized that the antagonistic activities of the LegK2/VipA effector pair can temporally control actin polymerization on the LCV to interfere with phagosome maturation and endosome recycling. Indeed, the VipA-induced actin polymerization "compensated" by LegK2 inhibition activity, or alternatively the actin polymerization inhibition activity exerted by LegK2 followed by the actin polymerization activity exerted by VipA, would be consistent with the well-established observation that, after bacterial engulfment, actin and associated proteins dissemble from the LCV but are recruited again at a later stage of endocytic transit [30, 52, 53]. In addition to directly controlling actin polymerization, *L. pneumophila* also controls actin degradation at the LCV [54] and secretes RavK, an actin-targeting effector protease. To achieve a comprehensive model of host actin cytoskeleton manipulation by *L. pneumophila*, the full set of 5 effectors known to interfere with actin polymerization (LegK2, VipA, Ceg14, RavK, and WipA) must be considered, and functional interactions between them will be studied in more detail.

5. Conclusion

The delivery of effector proteins that hijack host cell processes for the benefit of the bacteria is a mechanism widely used by bacterial pathogens and thus plays a key role in microbial virulence. *L. pneumophila*, which translocates a record number of 300 effectors, is the paradigm of a pathogen that has evolved a highly sophisticated relationship with its hosts and a perfect model to study the complex action of effectors and their functional interactions. Here, we revealed a new type of effector-effector suppression pair in *L. pneumophila*, which neither meets the emerging definition of a metaeffector, i.e., an effector that controls the activity of another effector, nor the new definition of a paraeffector, i.e., two effectors that act synergistically or oppositely on the same cellular target. Instead, LegK2 and VipA express their actin polymerization antagonistic activities by targeting two distinct cellular targets through two different molecular mechanisms, in order to finely control actin polymerization on the LCV surface. Importantly, their combined actions play a key role in the escape of bacteria from endocytic degradation and subsequent intracellular bacterial replication.

Data Availability

RNA-seq and sequencing data have been deposited in the European Nucleotide Archive database at EMBL-EBI (https://www.ebi.ac.uk/ena) under accession number PRJEB62121.

Conflicts of Interest

The authors declare no conflict of interest.

Authors' Contributions

P.D. designed the research; M.P., C.M., and N.B. performed experimental research, except proteomics; L.A. and K.P. designed, performed, and analyzed proteomics; M.P., J.B., E.K., and V.D. designed, performed, and analyzed evolutionary biology. M.P., C.M., N.B., O.D., and P.D. analyzed data; M.P. and P.D. wrote the paper. C. Michard and N. Baïlo contributed equally to this work.

Acknowledgments

We thank Adeline Page and Frédéric Delolme from the Protein Science Facility at the SFR Biosciences (UAR3444/CNRS, US8/Inserm, ENS de Lyon, UCBL) for the mass spectrometry analyses. We are grateful to F. Letourneur for the gift of anti-VatA antibody. We thank the Dicty Stock Center for *D. discoideum* strains. And finally, we thank Camille Fourneaux (LBMC, ENS de Lyon) for helping with R scripts. This work was funded by the Centre National de la Recherche Scientifique (UMR 5308), the Institut National de la Recherche Médicale (U1111), and the Université Lyon 1. The work of L.A. and K.P. was supported by a grant from Agence Nationale de la Recherche attributed to L.A. (Project RNAchap, ANR-17-CE11-0009-01). The Ph.D. grants to M.P., C.M., J.B., and O.D. were provided by the Ministère de l'Enseignement supérieur et de la Recherche.

Supplementary Materials

Supplementary Data S1: list of all cells and bacteria strains used in this study. Supplementary Data S2: list of plasmids used in this study. Supplementary Data S3: list of oligonucleotides used to realize mutant strains of *Legionella* as well as for cloning. Supplementary Data S4: accession numbers of genomes used for evolutionary analyses. Supplementary Data S5: Fasta files of sequencing data of *ΔlegK2* and *ΔlegK2*/*ΔvipA Legionella pneumophila* strains. Supplementary Data S6: axenic growth kinetics of *L. pneumophila* Paris WT, *ΔdotA*, *ΔlegK2*, *ΔvipA*, *ΔlegK2*/*ΔvipA*, mutant strains transformed with mCherry-expressing plasmids. Supplementary Data S7: luminescence emission from chromosomal translational fusions of *vipA::luc* (A) and *legK2::luc* (B) in *L. pneumophila* Paris strain grown in AYE medium at 30°C. Supplementary Data S8: mass spectrometry data following protein expression in *Legionella pneumophila* Paris WT at OD_{600nm} 1, 2, 3, 4, and 5. Supplementary Data S9: phylogenetic tree representing the phylogenetic diversity of *Legionella* genomes displaying either LegK2 (blue-green squares) or VipA genes (purple squares). *(Supplementary Materials)*

References

[1] T. E. B. Stradal, K. Rottner, A. Disanza, S. Confalonieri, M. Innocenti, and G. Scita, "Regulation of actin dynamics by WASP and WAVE family proteins," *Trends in Cell Biology*, vol. 14, no. 6, pp. 303–311, 2004.

[2] D. Truong, J. W. Copeland, and J. H. Brumell, "Bacterial subversion of host cytoskeletal machinery: hijacking formins and the Arp2/3 complex," *BioEssays*, vol. 36, no. 7, pp. 687–696, 2014.

[3] M. Pillon and P. Doublet, "Myosins, an underestimated player in the infectious cycle of pathogenic bacteria," *International Journal of Molecular Sciences*, vol. 22, no. 2, article E615, p. 615, 2021.

[4] J. Pizarro-Cerdá and P. Cossart, "*Listeria monocytogenes*: cell biology of invasion and intracellular growth," *Microbiology Spectrum*, vol. 6, no. 6, pp. 6–6, 2018.

[5] J. H. Lee, H. Park, and Y. H. Park, "Molecular mechanisms of host cytoskeletal rearrangements by Shigella invasins," *International Journal of Molecular Sciences*, vol. 15, no. 10, pp. 18253–18266, 2014.

[6] C. V. Da Silva, L. Cruz, A. N. da Silva et al., "A glance at *Listeria* and *Salmonella* cell invasion: different strategies to promote host actin polymerization," *International Journal of Medical Microbiology*, vol. 302, no. 1, pp. 19–32, 2012.

[7] G. Keb, J. Ferrell, K. R. Scanlon, T. J. Jewett, and K. A. Fields, "Chlamydia trachomatis TmeA directly activates N-WASP to promote actin polymerization and functions synergistically with TarP during invasion," *mBio*, vol. 12, no. 1, article e02861, 2021.

[8] M. D. Welch and M. Way, "Arp2/3-mediated actin-based motility: a tail of pathogen abuse," *Cell Host & Microbe*, vol. 14, no. 3, pp. 242–255, 2013.

[9] E. Weddle and H. Agaisse, "Principles of intracellular bacterial pathogen spread from cell to cell," *PLoS Pathogens*, vol. 14, no. 12, article e1007380, 2018.

[10] A. Heggie, O. Cerny, and D. W. Holden, "SteC and the intracellularSalmonella-induced F-actin meshwork," *Cellular Microbiology*, vol. 23, no. 4, Article ID e13315, 2021.

[11] Y. Kumar and R. H. Valdivia, "Actin and intermediate filaments stabilize the chlamydia trachomatis vacuole by forming dynamic structural scaffolds," *Cell Host & Microbe*, vol. 4, no. 2, pp. 159–169, 2008.

[12] W. L. Lee, J. M. Grimes, and R. C. Robinson, "Yersinia effector YopO uses actin as bait to phosphorylate proteins that regulate actin polymerization," *Nature Structural & Molecular Biology*, vol. 22, no. 3, pp. 248–255, 2015.

[13] K. Aktories, M. Bärmann, I. Ohishi, S. Tsuyama, K. H. Jakobs, and E. Habermann, "Botulinum C2 toxin ADP-ribosylates actin," *Nature*, vol. 322, no. 6077, pp. 390–392, 1986.

[14] I. S. Franco, N. Shohdy, and H. A. Shuman, "The legionella pneumophila effector VipA is an actin nucleator that alters host cell organelle trafficking," *PLoS Pathogens*, vol. 8, no. 2, article e1002546, 2012.

[15] Z. Guo, R. Stephenson, J. Qiu, S. Zheng, and Z.-Q. Luo, "A legionella effector modulates host cytoskeletal structure by inhibiting actin polymerization," *Microbes and Infection*, vol. 16, no. 3, pp. 225–236, 2014.

[16] C. Michard, D. Sperandio, N. Baïlo et al., "The *Legionella* kinase LegK2 targets the ARP2/3 complex to inhibit actin nucleation on phagosomes and allow bacterial evasion of the late endocytic pathway," *mBio*, vol. 6, article e00354, 2015.

[17] Y. Liu, W. Zhu, Y. Tan, E. S. Nakayasu, C. J. Staiger, and Z.-Q. Luo, "A Legionella effector disrupts host cytoskeletal structure by cleaving actin," *PLoS Pathogens*, vol. 13, no. 1, article e1006186, 2017.

[18] L. He, Y. Lin, Z.-H. Ge et al., "TheLegionella pneumophilaeffector WipA disrupts host F-actin polymerisation by hijacking phosphotyrosine signalling," *Cellular Microbiology*, vol. 21, no. 6, Article ID e13014, 2019.

[19] M. L. Urbanus, A. T. Quaile, P. J. Stogios et al., "Diverse mechanisms of metaeffector activity in an intracellular bacterial pathogen, Legionella pneumophila," *Molecular Systems Biology*, vol. 12, no. 12, p. 893, 2016.

[20] M. Z. Li and S. J. Elledge, "SLIC: a method for sequence- and ligation-independent cloning," *Methods in Molecular Biology*, vol. 852, pp. 51–59, 2012.

[21] N. Bailo, H. Kanaan, E. Kay, X. Charpentier, P. Doublet, and C. Gilbert, "Scar-free genome editing in Legionella pneumophila," *Methods in Molecular Biology*, vol. 1921, pp. 93–105, 2019.

[22] I. Durieux, C. Ginevra, L. Attaiech et al., "Diverse conjugative elements silence natural transformation in Legionella species," *Proceedings of the National Academy of Sciences of the United States of America*, vol. 116, no. 37, pp. 18613–18618, 2019.

[23] L. Attaiech, A. Boughammoura, C. Brochier-Armanet et al., "Silencing of natural transformation by an RNA chaperone and a multitarget small RNA," *Proceedings of the National Academy of Sciences of the United States of America*, vol. 113, no. 31, pp. 8813–8818, 2016.

[24] M. Steinegger and J. Söding, "MMseqs2 enables sensitive protein sequence searching for the analysis of massive data sets," *Nature Biotechnology*, vol. 35, no. 11, pp. 1026–1028, 2017.

[25] K. Katoh, J. Rozewicki, and K. D. Yamada, "MAFFT online service: multiple sequence alignment, interactive sequence choice and visualization," *Briefings in Bioinformatics*, vol. 20, pp. 1160–1166, 2019.

[26] M. N. Price, P. S. Dehal, and A. P. Arkin, "FastTree 2 – approximately maximum-likelihood trees for large alignments," *PLoS One*, vol. 5, no. 3, article e9490, 2010.

[27] F. Menardo, C. Loiseau, D. Brites et al., "Treemmer: a tool to reduce large phylogenetic datasets with minimal loss of diversity," *BMC Bioinformatics*, vol. 19, no. 1, p. 164, 2018.

[28] M. Csurös, "Count: evolutionary analysis of phylogenetic profiles with parsimony and likelihood," *Bioinformatics*, vol. 26, no. 15, pp. 1910–1912, 2010.

[29] I. Letunic and P. Bork, "Interactive tree of life (iTOL) v5: an online tool for phylogenetic tree display and annotation," *Nucleic Acids Research*, vol. 49, no. W1, pp. W293–W296, 2021.

[30] H. Lu and M. Clarke, "Dynamic properties of Legionella-containing phagosomes in Dictyostelium amoebae," *Cellular Microbiology*, vol. 7, no. 7, pp. 995–1007, 2005.

[31] E. Hervet, X. Charpentier, A. Vianney et al., "Protein kinase LegK2 is a type IV secretion system effector involved in endoplasmic reticulum recruitment and intracellular replication of Legionella pneumophila," *Infection and Immunity*, vol. 79, no. 5, pp. 1936–1950, 2011.

[32] T. Sahr, C. Rusniok, D. Dervins-Ravault, O. Sismeiro, J.-Y. Coppee, and C. Buchrieser, "Deep sequencing defines the transcriptional map of L. *pneumophila* and identifies growth phase-dependent regulated ncRNAs implicated in virulence," *RNA Biology*, vol. 9, pp. 503–519, 2012.

[33] X. Charpentier and E. Oswald, "Identification of the secretion and translocation domain of the enteropathogenic and EnterohemorrhagicEscherichia colieffector Cif, using TEM-1 β-lactamase as a new fluorescence-based reporter," *Journal of Bacteriology*, vol. 186, no. 16, pp. 5486–5495, 2004.

[34] X. Charpentier, J. E. Gabay, M. Reyes, J. W. Zhu, A. Weiss, and H. A. Shuman, "Chemical genetics reveals bacterial and host cell functions critical for type IV effector translocation by legionella pneumophila," *PLoS Pathogens*, vol. 5, no. 7, article e1000501, 2009.

[35] J. Allombert, C. Jaboulay, C. Michard et al., "Deciphering legionella effector delivery by Icm/Dot secretion system reveals a new role for c-di-GMP signaling," *Journal of Molecular Biology*, vol. 433, no. 13, article 166985, 2021.

[36] J. N. Bugalhão, L. J. Mota, and I. S. Franco, "Identification of regions within the Legionella pneumophila VipA effector protein involved in actin binding and polymerization and in interference with eukaryotic organelle trafficking," *Microbiology Open*, vol. 5, no. 1, pp. 118–133, 2016.

[37] J. Schmölders, C. Manske, A. Otto et al., "Comparative proteomics of purified pathogen vacuoles correlates intracellular replication of Legionella pneumophila with the small GTPase Ras-related protein 1 (Rap1)," *Molecular & Cellular Proteomics*, vol. 16, no. 4, pp. 622–641, 2017.

[38] D. Burstein, F. Amaro, T. Zusman et al., "Genomic analysis of 38 Legionella species identifies large and diverse effector repertoires," *Nature Genetics*, vol. 48, no. 2, pp. 167–175, 2016.

[39] S. R. Shames, L. Liu, J. C. Havey, W. B. Schofield, A. L. Goodman, and C. R. Roy, "Multiple Legionella pneumophila effector virulence phenotypes revealed through high-throughput analysis of targeted mutant libraries,"

Proceedings of the National Academy of Sciences of the United States of America, vol. 114, no. 48, pp. E10446–E10454, 2017.

[40] T. Kubori, N. Shinzawa, H. Kanuka, and H. Nagai, "Legionella metaeffector exploits host proteasome to temporally regulate cognate effector," *PLoS Pathogens*, vol. 6, no. 12, article e1001216, 2010.

[41] M. R. Neunuebel, Y. Chen, A. H. Gaspar, P. S. Backlund, A. Yergey, and M. P. Machner, "De-AMPylation of the small GTPase Rab1 by the pathogen Legionella pneumophila," *Science*, vol. 333, no. 6041, pp. 453–456, 2011.

[42] Y. Tan and Z.-Q. Luo, "Legionella pneumophila SidD is a deAMPylase that modifies Rab1," *Nature*, vol. 475, no. 7357, pp. 506–509, 2011.

[43] Y. Tan, R. J. Arnold, and Z.-Q. Luo, "Legionella pneumophila regulates the small GTPase Rab1 activity by reversible phosphorylcholination," *Proceedings of the National Academy of Sciences of the United States of America*, vol. 108, no. 52, pp. 21212–21217, 2011.

[44] J. C. Havey and C. R. Roy, "Toxicity and SidJ-mediated suppression of toxicity require distinct regions in the SidE family of Legionella pneumophila effectors," *Infection and Immunity*, vol. 83, no. 9, pp. 3506–3514, 2015.

[45] K. C. Jeong, J. A. Sexton, and J. P. Vogel, "Spatiotemporal regulation of a Legionella pneumophila T4SS substrate by the metaeffector SidJ," *PLoS Pathogens*, vol. 11, no. 3, article e1004695, 2015.

[46] A. M. Joseph, A. E. Pohl, T. J. Ball et al., "The Legionella pneumophila metaeffector Lpg2505 (MesI) regulates SidI-mediated translation inhibition and novel glycosyl hydrolase activity," *Infection and Immunity*, vol. 88, no. 5, article e00853, 2020.

[47] D. Valleau, A. T. Quaile, H. Cui et al., "Discovery of ubiquitin deamidases in the pathogenic arsenal of Legionella pneumophila," *Cell Reports*, vol. 23, no. 2, pp. 568–583, 2018.

[48] A. McCloskey, K. Perri, T. Chen, A. Han, and Z.-Q. Luo, "The metaeffector MesI regulates the activity of the Legionella effector SidI through direct protein-protein interactions," *Microbes and Infection*, vol. 23, no. 4-5, p. 104794, 2021.

[49] D. Schator, S. Mondino, J. Berthelet et al., "Legionella para-effectors target chromatin and promote bacterial replication," *Nature Communications*, vol. 14, no. 1, p. 2154, 2023.

[50] N. Shohdy, J. A. Efe, S. D. Emr, and H. A. Shuman, "Pathogen effector protein screening in yeast identifies Legionella factors that interfere with membrane trafficking," *Proceedings of the National Academy of Sciences of the United States of America*, vol. 102, no. 13, pp. 4866–4871, 2005.

[51] L. Toulabi, X. Wu, Y. Cheng, and Y. Mao, "Identification and structural characterization of a Legionella phosphoinositide phosphatase," *The Journal of Biological Chemistry*, vol. 288, no. 34, pp. 24518–24527, 2013.

[52] J. H. Vines and J. S. King, "The endocytic pathways of Dictyostelium discoideum," *The International Journal of Developmental Biology*, vol. 63, no. 8-9-10, pp. 461–471, 2019.

[53] N. Capitani and C. T. Baldari, "F-actin dynamics in the regulation of endosomal recycling and immune synapse assembly," *Frontiers in Cell and Developmental Biolog*, vol. 9, article 670882, 2021.

[54] O. Shevchuk, C. Batzilla, S. Hägele et al., "Proteomic analysis of legionella-containing phagosomes isolated from Dictyostelium," *International Journal of Medical Microbiology*, vol. 299, no. 7, pp. 489–508, 2009.